Chapter 5
Beyond Intercalation: Nanoscale-Enabled Conversion Anode Materials for Lithium-Ion Batteries

Fabrice M. Courtel, Hugues Duncan, and Yaser Abu-Lebdeh

Abstract The use of transition metal oxides as anode materials in lithium-ion batteries offers great advantages over graphitic carbon due to their ability to deliver much higher specific capacities. The mechanism with which they electrochemically react with lithium was found to be peculiar and termed "conversion" to distinguish it from other mechanisms such as intercalation, insertion, and alloying. In this chapter, we have reviewed the behavior of a wide variety of transition metal oxides in lithium-ion batteries and the effect of structure/property relationship on their performance. It was found that a key enabler to the electrochemical reactivity of transition metal oxides is the nanosize effect and essentially the formation of nanoparticles and nanocomposites.

5.1 Introduction

In the recent years, there has been an increasing demand for high-power lithium-ion batteries (LIBs) for applications in portable electronics, plug-in hybrid vehicles (PHEVs), and other electric vehicles (EVs). While many new high-voltage and/or safer positive electrode (referred to as cathode) materials have been successfully developed and commercialized in the last years, such as carbon-coated nano-$LiFePO_4$, [1–3] $LiNi_{1/3}Co_{1/3}Mn_{1/3}O_2$ [4, 5], and $LiNi_{0.8}Co_{0.15}Al_{0.05}O_2$ [5, 6], the replacement of the carbon graphite negative electrode (referred to as anode) has been relatively less successful. Graphite has a high electronic conductivity

F.M. Courtel
Atomic Energy of Canada Limited, Chalk River, ON K0J 1J0, Canada

H. Duncan
Lawrence Berkeley National Laboratory, Berkeley, CA 94720, USA

Y. Abu-Lebdeh (✉)
National Research Council of Canada, Ottawa, ON K1A 0R6, Canada
e-mail: Yaser.Abu-Lebdeh@nrc.gc.ca

Y. Abu-Lebdeh and I. Davidson (eds.), *Nanotechnology for Lithium-Ion Batteries*, Nanostructure Science and Technology, DOI 10.1007/978-1-4614-4605-7_5,
© Springer Science+Business Media, LLC 2013

(σ_a: 2.6 × 10^4 S cm^{-1} and σ_c: 2 × 10^2 S cm^{-1} [7]), is not too costly, and has a good capacity retention and very good cycle life. However, it is limited by its theoretical gravimetric and volumetric capacities: 372 mAh g^{-1} and 830 mAh mL^{-1}, respectively. Recently, Sony has prompted an interest in the Sn-Co-C alloy composite anode [8–15] and is now manufacturing this new generation of LIBs called Nexelion™ [16]. This battery leads to much higher gravimetric and volumetric capacities but to a lower long-term reversibility compared to graphite. Sony reported a capacity increase of about 30% compared to their conventional battery, good rate capability, and good temperature performance [8]. Others, such as Toshiba, chose a safer and "zero-strain" [17] insertion anode material, the nano-$Li_4Ti_5O_{12}$ (a.k.a. LTO) [18–21] in the super-charge ion battery (SCiB™) with an output voltage of 2.4 V. LTO has a very good cycle life and high rate capability that allows quick charges/discharges [22], which is of interest for PHEV applications [18]. In addition, its high delithiation voltage (1.5 V vs. Li/Li^+) makes it safer than other anode materials [18–21]; indeed, there is no risk of lithium plating and presumably no SEI formation. However, its drawback is the low theoretical specific capacity (175 mAh g^{-1}/612 mAh mL^{-1}) and high lithium insertion voltage. Another alternative to the common anode material is to use elements, preferably nanometric in size, that can alloy with lithium, such as aluminum, silicon, or tin; they provide high specific capacities usually ranging from 1,000 to 4,000 mAh g^{-1} (2,700 to 9,800 mAh mL^{-1}). However, there is a large volume change between their unlithiated and their lithiated state: 100% for LiAl [23–25], 300–400% for Li_xSi (x = 3.5 or 4.2) [23, 26–29], and 260% for $Li_{4.4}Sn$ [23, 30, 31]. That gives rise to mechanical stresses that lead to cracks, eventual disintegration of the electrode, and failure of the LIB [32]. The use of nanoparticles [29] or nanocomposites [33] that can provide faster stress relaxations along with a binder that can accommodate the volume change, such as sodium carboxymethyl cellulose [34] or styrene-butadiene rubber [35], usually mitigate this issue. In addition, it is widely accepted now that anode materials that are prone to large volume changes during battery cycling warrant the use of ionic polymeric binders instead of conventional PVDF. This leads to better performance by allowing better lithium-ion transport from the electrolyte to the particles of the active material, more uniform coverage of the binder to the surface of the particles, and more uniform SEI formation at the surface of the particles [36]. In the last decade, transition metal oxides (TMOs), sulfides (TMSs), nitrides (TMNs), phosphides (TMPs), or fluorides (TMFs) (also referred as TMXs) have shown their potential as the next generation of anode materials for LIBs. Despite the fact that TMXs, with TM having the lowest oxidation number (e.g., Fe^{2+}, Mn^{2+}), lack interstitial sites for lithium insertion and the fact that none of these 3d transition metals (TMs) alloy with lithium, they happen to be active toward lithium [37, 38]. As shown by Fig. 5.1, TMOs provide capacities ranging from 650 to 1,000 mAh g^{-1} (3,300 to 5,000 mAh mL^{-1}) which is two to three times higher than graphite. However, the delithiation potential of these materials is higher than graphite, typically between 1.2 and 2.5 V versus Li/Li^+.

This chapter exposes the processes by which TMXs can be reversibly lithiated and delithiated and the factors that influence their performance, such as capacity

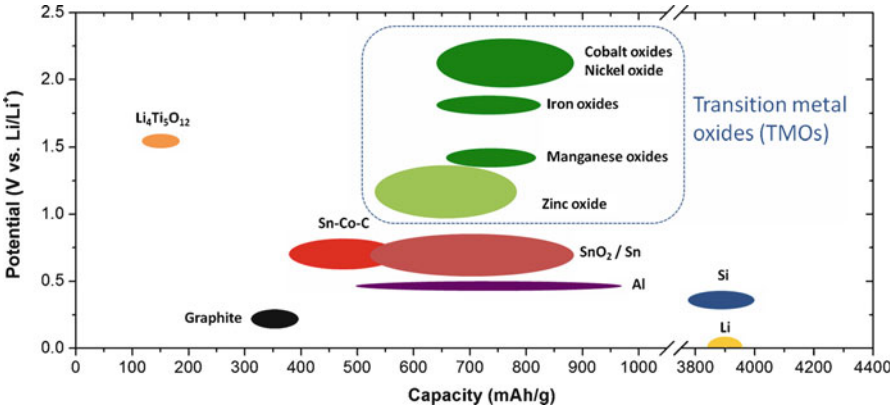

Fig. 5.1 Delithiation potential versus gravimetric specific capacity of anode materials

values, rate capability, and capacity retention. The discussion is mainly focused on TMOs going from chromium oxide to zinc oxide, and from simple oxides to mixed oxides such as spinel AB_2O_4. The last part of this chapter goes over the other TMXs introduced above.

5.2 Lithiation and Delithiation Mechanism

The use of TMOs as anode materials for LIBs is recent, but their use as cathode materials is not new: Li-CuO primary cells have been in use since 1980 [39, 40], and more recently, CuO has been used as a cathode material [41]. At room temperature, the simplified and nonreversible reaction was believed to be Eq. 5.1 with Cu_2O as an intermediate:

$$CuO + 2Li^+ + 2e^- \rightarrow Cu + Li_2O \tag{5.1}$$

The experimental cell voltage was about 1.5 V versus Li/Li^+ [39]. Even though in 1981 it has already been shown that the reaction of Fe_2O_3/Fe_3O_4 with lithium was reversible at 420°C [42], it was only in 2000 that Poizot et al. demonstrated that this reaction could be reversible at room temperature [37].

Unlike graphite, $Li_4Ti_5O_{12}$, or cathode materials which undergo a reversible intercalation/insertion reaction with Li^+, most TMXs go through a reversible conversion reaction with Li^+. While for the intercalation/insertion process less than one electron per metal is transferred (≈0.5 for $LiCoO_2$, 1 for $LiFePO_4$, 0.6 for $Li_4Ti_5O_{12}$, and 0.17 for graphite), for the conversion reaction, often a transfer of more than two electrons per metal occurs. As shown by Eq. 5.2, during the lithiation

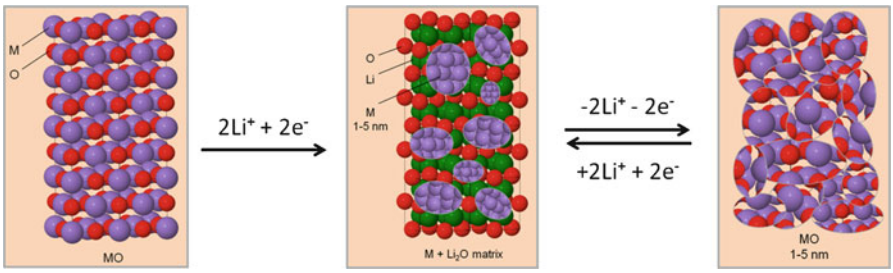

Fig. 5.2 Reversible conversion reaction of MO with lithium

step of the conversion reaction, the TMO is reduced into its metallic state and a decomposable matrix of Li_2O is formed:

$$MO_x + 2xLi^+ + 2xe^- \leftrightarrow M + xLi_2O \tag{5.2}$$

As shown by Fig. 5.2, after the first lithiation, a composite made of metal nanoparticles (typically 1–5 nm) embedded into a Li_2O matrix is formed [37]. During the delithiation process, nanoparticles of the metal oxide (typically 1–5 nm) are formed back, however, not necessarily with the same crystalline structure as the starting oxide. The same conversion reaction occurs with SnO_2 [43] and Sb_2O_3 [44]; however, in these cases, the Li_2O matrix is not decomposable and the subsequent process with lithium will be a reversible alloying reaction between lithium and tin or lithium and antimony. The reversible conversion reaction with lithium is not unique to TMOs; indeed, TMSs, TMNs, TMPs, and TMFs undergo the same reaction. The reaction can be generalized as:

$$MX_y + zLi^+ + ze^- \leftrightarrow M + zLiX_{y/z(y=z \text{ for } X=F; y=z/2 \text{ for } X=O, S; y=z/3 \text{ for } X=N, P)} \tag{5.3}$$

The theoretical cell voltage (E) of a half-cell, using lithium metal as counter electrode, is calculated from the Gibbs free energy of formation of the metal oxide nanoparticle and the decomposable Li_2O matrix (ΔG_f) using the Nernst equation shown in Eq. 5.4 [45]. (E is also known as the electromotive force, emf):

$$\Delta G_f = -nFE \tag{5.4}$$

where n is the number of electron exchanged, F the Faraday constant, and E the theoretical cell voltage also known as the electromotive force (emf). ΔG_f is easily calculated using Eq. 5.5:

$$\Delta G_f = n\Delta G_f^\circ(Li_2O) - \Delta G_f^\circ(MO) \tag{5.5}$$

Table 5.1 Theoretical half-cell voltages (E or emf) calculated using the Gibbs free energy of formation ($\Delta_f G$) and theoretical specific capacities of several TMOs [45]

Metal oxide	E or emf (V vs. Li/Li^+)	Theoretical specific capacity (mAh g^{-1})
MgO	−0.00354	1,330
Al_2O_3	0.180	1,577
TiO_2 (rutile)	0.608	1,342
TiO_2 (anatase)	0.625	1,342
SiO_2	0.694	1,784
V_2O_3	0.945	1,073
MnO	1.032	756
Cr_2O_3	1.085	1,058
ZnO	1.252	659
Mn_2O_3	1.431	1,018
FeO	1.61	746
Fe_2O_3	1.631	1,007
MnO_2	1.708	1,233
CoO	1.802	715
NiO	1.954	718
Cu_2O	2.147	375
CuO	2.248	674

Theoretical half-cell voltages for a variety of metal oxides (sulfides, nitrides, and fluorides) and their theoretical specific capacities are shown in Table 5.1 [45].

These values assume that the metal will not alloy with Li, which is the case for all metals except silicon, aluminum, magnesium, and zinc. Furthermore, one should be aware that the Nernst equation is accurate for bulk material only, which means that the surface/interface energy contributions that become significant when nanoparticles are used have been neglected. Taking the latter into account would change the emf values by only 100 mV [45, 46]. Even though Al_2O_3, TiO_2, and SiO_2 exhibit a positive emf and thus their conversion reaction should be spontaneous, there are kinetic limitations that prevent the reaction from taking place. These oxides either are unreactive toward lithium, such as MgO and Al_2O_3, or undergo an insertion reaction, such as TiO_2.

The working potential (U) of the electrode in a half-cell is mostly determined by the emf and is also influenced by the lithiation or the delithiation overpotential (η) according to the following equation:

$$\mathrm{U} = \mathrm{emf} \pm \eta(-\text{if lithiation and} + \text{if delithiation}) \tag{5.6}$$

For TMOs that do react with lithium, a large overpotential is observed for both reactions (lithiation and delithiation) due to slow kinetics associated with solid-state reactions. Thus, a large potential window is usually required, typically 10 mV to 3 V versus Li/Li^+. Due to these kinetic limitations, only metal oxides that show an emf above 1 V versus Li/Li^+ have been experimentally proven to be reduced before the electrodeposition of lithium metal on the metal oxide occurs [45].

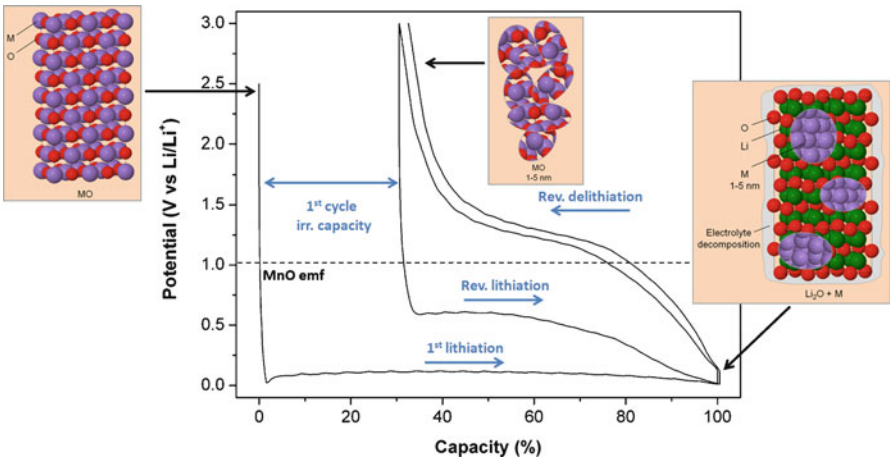

Fig. 5.3 Typical voltage profile of a half-cell made of a lithium metal counter electrode and a TMO working electrode (also applicable for TMSs, TMNs, TMPs, and TMFs). The half-cell was cycled between 10 mV and 3 V at 75 mA g^{-1}. Only the first two cycles are shown

TMXs, for which the metal is at its lowest oxidation state (e.g., MnO, FeO, CoO, NiO, Cu_2O, ZnO), directly undergo the reversible conversion reaction. However, in the case of a higher oxidation state and especially for compounds that exhibit a marked ionic character (i.e., TMOs and TMFs) or a covalent character (i.e., TMPs), due to the presence of vacancies, lithium insertion is going to occur before the reversible conversion reaction [38]. The lithium insertion induces the reduction of the TM to a lower oxidation state, and often, when the lowest (or the most stable) oxidation state is reached, the reversible conversion reaction occurs. Here are some examples of materials that follow this path: MnO_2 [47], Co_3O_4 [48, 49], Mn_3O_4 [50], CuO [51], CuS [52], Cu_3P[53], NiP_3 [54], Fe_2O_3 [55], and FeP [56].

The key point of the reversible conversion reaction of TMOs is the formation of nanoparticles of TM embedded and homogeneously distributed in a Li_2O matrix during the first lithiation. Figures 5.3 and 5.4 show typical voltage profiles of MnO, CoO, NiO, and FeO, respectively, as a function of the state of charge of the anode material in half-cell conditions.

MnO, FeO, CoO, and NiO all undergo a reversible conversion reaction, and their voltage profiles are very similar, except for the position of the lithiation and delithiation plateaus. As shown by Fig. 5.3, MnO exhibits a first lithiation plateau at 0.2 V versus Li/Li^+ where MnO particles are disintegrated into nanoparticles of manganese embedded into a Li_2O matrix. In this particular case, MnO particles were prepared by decomposition of manganese acetate at 800°C under argon. The working electrode composition is 80 wt% MnO, 5 wt% graphite, 5 wt% Super S carbon, and 10 wt% sodium carboxymethyl cellulose. In the case of CoO, starting from well crystallized CoO particle of 100–200 nm aggregated in grains of 1–2 μm (see Fig. 5.4a and b), after the first lithiation (plateau at 0.9 V vs. Li/Li^+), the

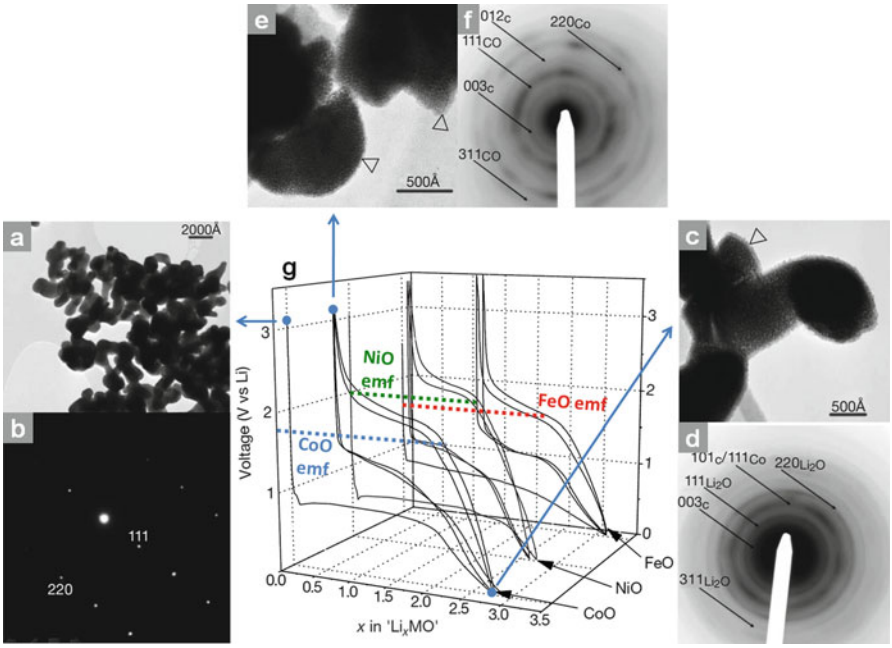

Fig. 5.4 (**a**) TEM micrograph of an uncycled CoO electrode with (**b**) its corresponding SAED patterns (taken along the [22-4] direction in the reciprocal space); (**c**) TEM micrograph of a fully lithiated CoO electrode, with (**d**) its corresponding SAED pattern (negative form); (**e**) TEM micrograph of a delithiated CoO electrode with (**f**) its corresponding SAED pattern (negative form); the subscript c in the hkl notation refers to carbon. (**g**) Voltage profile of a half-cell made of a lithium metal counter electrode and CoO, NiO, and FeO working electrodes, cycled between 0.01 and 3 V at a rate of C/5 (Reprinted by permission from Macmillan Publishers Ltd: Nature, [37], copyright 2011)

particles are totally disintegrated and are then composed of cobalt nanoparticles dispersed in Li_2O (see Fig. 5.4c and d). However, the overall shape of the starting particle/grain is preserved. The preservation of the shape has also been observed for carbon-coated Fe_3O_4 nanospindles [57] and three-dimensionally ordered mesoporous (3-DOM) Cr_2O_3 [58]. As shown in the scheme in Fig. 5.3, the electrode material is covered by a gel-like layer (also called organic layer, polymeric layer, or solid electrolyte interface); the empty triangle on Fig. 5.4c illustrates this layer. As mentioned before, a large overpotential is observed for TMOs; in the case of MnO, it is about 0.8 V, and for CoO, it is about 0.9 V. As explained by Poizot et al., it is believed that the size confinement of the TM nanoparticles enhances their electrochemical activity toward the decomposition of the Li_2O matrix [37]; a phenomenon explained by Maier in terms of a nano-effect resulting from increased surface energies of confined space [59]. The oxidation of the TM particles does not occur at a microscopic scale [37]; the particles must be nanometric and in close contact with Li_2O for this already slow solid-state oxidation reaction to occur [23].

Table 5.2 Summary table of electromotive forces, reduction and oxidation potentials, and theoretical capacities of TMOs ranging from chromium oxide to zinc oxide

TM	Phase	EMF[c] [45] (V)	E first reduction (V vs. Li/Li^+)	E second reduction (V vs. Li/Li^+)	E oxidation (V vs. Li/Li^+)	Number of Li per metal	Theoretical specific capacity [45] (mAh g^{-1})
Cr	Cr_2O_3	1.085	0.15 [60]	0.3–0.15[a] [60]	0.8–1.9[b] [60]	3	1,058
Mn	MnO_2	1.708	0.4[a] [61]	0.4–0.6[b] [61]	0.5–1.4[b][61]	4	1,233
	Mn_2O_3	1.431	1.4/0.35[a] [50]	0.6[b] [50]	1.0–1.4[b] [50]	3	1,018
	Mn_3O_4	–	1.1/0.4 [a] [50]	0.6 [50]	1–1.4[b] [50]	2.7	1,008
	MnO	1.032	0.2 [here]	0.5–0.6[b] [here]	1.0–1.4[b] [here]	2	756
Fe	Fe_2O_3	1.631	1.5/0.75[a] [62]	1.0/1.5[a][62]	1.5–2.0[b] [62]	3	1,007
	Fe_3O_4	–	0.7 [63]	0.8/1.0 [63]	1.5–2.0[b][63]	2.7	926
	FeO	1.61	0.6–0.7 [37]	0.9–1.1 [37]	1.5–1.8[b] [37]	2	746
Co	Co_3O_4	–	1.0 [48]	1.25 [48]	2.1 [48]	2.7	891
	CoO	1.802	1.0 [37]	1.2–1.8[b][37]	2.0–2.3[b][37]	2	715
Ni	NiO	1.954	0.6 [64]	1.0–1.4[b] [64]	1.5–2.2 [b] [64]	2	718
Cu	CuO	2.248	2.2/1.5/0.8 [65]	2.2/1.5/0.8 [66]	1.0–1.5/2.4 [65]	2	674
	Cu_2O	2.147	1.1–1.2 [67]	0–1.5[b] [67]	1.5[b]/2.5 [68]	1	375
Zn	ZnO	1.252	0.3–0.4 [69]	0.9–0.5[b] [70]	from 1.2 [70]	2	659

[a]2 plateaus
[b]Slope
[c]EMF: Electromotive force

As shown in Fig. 5.3, the delithiation plateau of MnO also shows the polarization of the electrode material; it ranges from 1.0 to 1.4 V versus Li/Li^+. In the case of CoO, the position of the plateau is much higher; it ranges between 1.8 and 2.1 V versus Li/Li^+. In general, the delithiation plateau is not affected by the cycle number because the metal-Li_2O composite is already at a nanoscale after the first lithiation. At the end of the delithiation, TMO nanoparticles are obtained, as shown by Fig. 5.4e and f. In most cases, subsequent lithiation plateaus show a much lower overpotential, due to the ease of reducing nanoparticles (1–5 nm) compared to bigger particles (≈100 nm). In the case of MnO, the overpotential of the second lithiation is only 0.4 V. However, as shown in Figs. 5.3 and 5.4, the reduction and oxidation overpotentials are responsible for the large hysteresis that negatively affects the efficiencies of the batteries. Similar effect was also observed in the case of TMXs. Table 5.2 summarizes the lithiation and delithiation potentials for different TMOs, with TMs ranging from chromium to zinc (zinc is included even though it is a post-transition metal).

The composition and the nature of the gel-like layer at the surface of the material vary with the state of lithiation; it is usually thicker when the material is lithiated

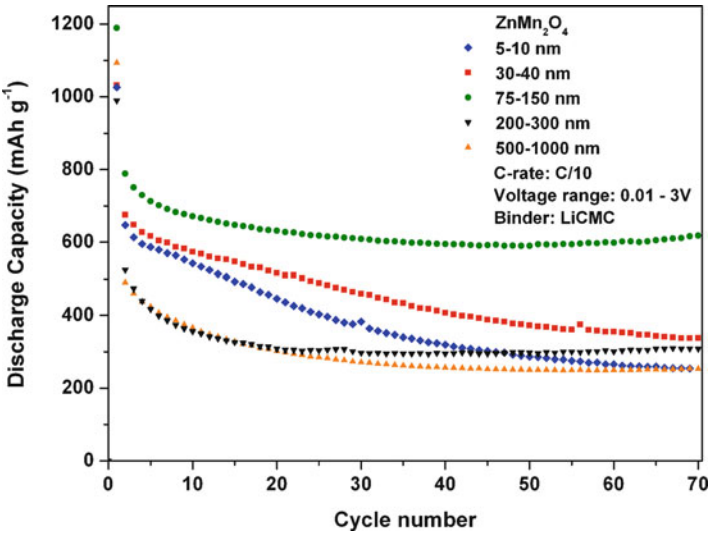

Fig. 5.5 Discharge capacities of $ZnMn_2O_4$ electrodes as a function of cycle number for electrodes made of particles of $ZnMn_2O_4$ having different sizes (size measured via TEM or SEM). Lithium carboxymethyl cellulose was used as binder and the electrodes tested in half-cells and cycled at C/10

which makes this layer unstable [50, 59, 60, 61]. In addition, this layer is known to grow with cycling time and with the increase of temperature and prolonged cycling [23]. Interestingly enough, this unstable layer is able to reversibly store lithium to some extent via an interfacial charging mechanism [45, 46, 72]. This storage capability has been observed for CoO [23] and also for other TMOs such as $ZnMn_2O_4$ [73]. The phenomenon is enhanced by an increase in temperature or prolonged cycling [23, 73].

Even though "nano" is the key point of the reversibility of the conversion reaction of TMOs (and TMXs in general), the capacity retention of these electrode materials is very sensitive to the particle size and morphology of the material. As shown by Poizot et al. in the case of CoO, an optimum particle size of 2 μm is observed, whereas for Cu_2O, it is 1 μm [37]. In the case of spherical particles of Co_3O_4, a crystallite size ranging between 40 and 60 nm seems to be the optimum [74, 75]. Figure 5.5 shows the battery performance of the spinel TMO $ZnMn_2O_4$ prepared via a coprecipitation method [73]. In this particular case, electrodes made of particles of $ZnMn_2O_4$ having a size of 75–150 nm show the highest and the most stable capacity at 690 mAh g^{-1} after 70 cycles [73].

Recently, Maier has suggested a new mechanism for interfacial ion storage at the nanoscale level [76]. This was illustrated in lithium-ion batteries by a study of the storage mechanism in nano-RuO_2 (30–200 nm) where high capacities reaching 1,110 mAh g^{-1} were obtained at unusually high coulombic efficiencies reaching 98% [72]. It was shown that lithium ions can be stored at the interface of the

Ru/Li_2O nanocomposite (between 0 and 1.2 V) with capacities reaching 120 mAh g^{-1} at C/5. The Ru/Li_2O nanocomposite was formed by a conversion reaction prior to an intercalation reaction that formed $LiRuO_2$. The formation of a SEI (5 nm) was observed during charging, similar to other metal oxides (e.g., CoO), but it was suggested to be less plausible in this case because of its formation and dissolution at a different potential above 1.2 V [77]. The storage at the M/Li_2O interface was explained to be capacitive-like in nature where lithium ions occupy interstitial sites in Li_2O close to the boundary compensated by the electron sitting on the metal surface site. A similar mechanism was suggested to take place for a Ti/Li_2O nanocomposite as shown by ab initio calculations [77].

5.3 Metal Oxides

This section presents the properties and performance of TMOs which undergo a reversible conversion reaction with lithium. TMOs go from chromium oxide to zinc oxide, and all potentials are given versus Li/Li^+.

5.3.1 Chromium

According to the emf calculations reported by Maier et al. [45], Cr_2O_3 is the first TMOs from the periodic table which undergoes a conversion reaction with lithium [60] but also means that it is one of the most difficult to reduce. The first lithiation shows a plateau at 0.15 and at 0.3 V for the subsequent lithiations, whereas the delithiation potential ranges from 0.8 to 1.9 V [60]. Even though Cr_2O_3 has a large theoretical specific capacity of 1,058 mAh g^{-1}, micrometric particles always show very poor capacity retention. Particles with size that ranges from 500 nm to 1.5 μm show a first discharge capacity of 1,100 mAh g^{-1}, which is slightly higher than the theoretical capacity. Unfortunately, the second cycle usually shows a specific capacity of 250 mAh g^{-1} or less [60]. Even using nanoparticles (50 nm) prepared via a hydrothermal method is not sufficient to improve significantly the capacity retention and the long-term performance of the electrode [60]. At first, it seemed that this poor capacity was due to the conversion reaction mechanism, which was believed to proceed, according to Dupont et al., as follows: $Cr_2O_3 \rightarrow CrO \leftrightarrow Cr \leftrightarrow CrO$ [78]. Cr_2O_3 was prepared using a pulsed laser deposition technique that produced particles of 50 nm and more in size. In this case, no Cr_2O_3 crystalline phase was observed after the first cycle. However, other groups observed the recovery of Cr_2O_3 after the delithiation [60]. It is worth mentioning that one of the main issues with Cr_2O_3 is its poor electronic conductivity ($\approx 2 \times 10^{-7}$ S cm^{-1}) [71]. This observation applies for all TMOs which exhibit typical insulator or semiconductor behavior with their bandgaps ranging from 3 to 4 eV [79]. In addition, the formation of a very thick and unstable gel-like layer of 30–90 nm

on the surface of the nanoparticles is responsible for a capacity loss of about 250 mAh g^{-1} [60]. These issues have been circumvented by making a carbon/Cr_2O_3 nanocomposite coated with hard carbon; it provided a reversibility of 80%. The reported capacity values are 800 mAh g^{-1} (per gram of composite) for the first cycle and a reversible capacity of 650 mAh g^{-1} after 20 cycles [60, 80]. However, long-term cycling performance has not been reported yet. Doping was another path that has been investigated in order to overcome the low electronic conductivity. Carbon-coated Cr_2O_3 nanoparticles which were previously doped with 2% of Ni have shown a reversibility of almost 90% with an initial capacity of 900 mAh g^{-1} and a reversible capacity of 800 mAh g^{-1} after 20 cycles [71]. The doping increased the electronic conductivity from 2×10^{-7} S cm^{-1} to 3×10^{-4} S cm^{-1}, and the carbon coating improved the stability of the gel-like layer by decreasing its thickness from 30–90 nm to 15–30 nm [60, 71]. More recently, 3-DOM Cr_2O_3 made of 10-nm thick walls and 10-nm pores was successfully prepared, but unfortunately, the lack of electrical conductivity and of carbon coating leads to very poor performance [58]. Other strategies have been investigated, such as 100–200-nm thin films [81] or the growth of a 500-nm porous layer of Cr_2O_3/Mn-Fe-Cr-O directly onto stainless steel [78, 81]. However, these strategies greatly diminished the capacity density of the electrodes.

5.3.2 Manganese

Four different manganese oxides are available as anode material for lithium-ion batteries, ranging from Mn^{4+} to Mn^{2+}: MnO_2 [47], Mn_2O_3 [82, 83], Mn_3O_4 [83, 84], and MnO [50, 61, 86–89]. As shown by Table 5.2, they all show high theoretical capacities, starting from 1,233 mAh g^{-1} for MnO_2 to 755 mAh g^{-1} for MnO, which are four to two times greater than graphite. Manganese is an appealing metal; it is not too expensive, abundant, and nontoxic. In addition, the delithiation (oxidation) potential is quite low compared to other TMOs (see Table 5.2). However, the main issue with manganese is the irreversible capacity associated with the first cycle. Like Cr_2O_3, manganese oxides are the most difficult TMOs to reduce; a potential of about 0.2–0.4 V is usually needed [38]. An interesting study was done by Fang et al. that compared the behavior of the four manganese oxides having the same nanorod morphology with a diameter ranging from 100 to 200 nm [50]. Figure 5.6 shows the SEM micrographs and the voltage profiles of these four oxides. The irreversible capacity represents 71.8% for MnO_2, 58.26% for Mn_2O_3, 52.7% for Mn_3O_4, and 45% for MnO.

As previously mentioned, MnO_2 goes through a lithium insertion process before being reduced to manganese metal according to the following path: $MnO_2 \leftrightarrow LiMnO_2 \rightarrow Li_2MnO_2 \rightarrow Mn$ [50, 90]. The large irreversible capacity is explained by the nonreversibility of some of these reactions. Mn_2O_3 is irreversibly reduced into Mn_3O_4 before being further reduced. MnO_2 and Mn_2O_3 do not usually show good capacity retention. The third manganese oxide, Mn_3O_4, goes through an insertion

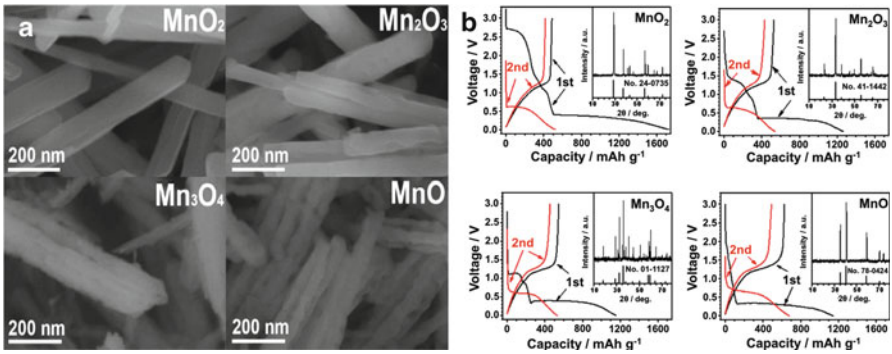

Fig. 5.6 (**a**) SEM micrographs and (**b**) voltage profile of MnO_2, Mn_2O_3, Mn_3O_4, and MnO nanorods prepared via the same method (Reprinted from Electrochemistry Communications [50]. Copyright (2011), with permission from Elsevier)

reaction before being reduced to manganese metal: $Mn_3O_4 \rightarrow LiMn_3O_4 \rightarrow MnO \leftrightarrow Mn$. After the different insertion steps, all manganese oxides show the same first reduction voltage plateau at 0.2–0.4 V, typical of the conversion reaction. An advantage with using manganese oxides is the low voltage of the oxidation plateau of the conversion reaction that ranges from 1.0 to 1.4 V; this allows a higher output cell voltage. Two different reversible processes with lithium have been reported in the literature for Mn_3O_4 [50, 84]. According to Fang et al., first an insertion of lithium occurs to form $LiMn_3O_4$ as shown by Eq. 5.6. A second reaction with lithium then takes place to obtain MnO, as shown by Eq. 5.7. It has been shown that once MnO is obtained, reactions (5.6) and (5.7) are not reversible anymore. From MnO, the reversible conversion reaction occurs, as shown by Eq. 5.8; the latter observation has been demonstrated by high-resolution TEM and selected area electron diffraction (SAED) measurements [50]. A second path has also been proposed by Gao et al. where they state that reaction shown by Eq. (5.9) is totally reversible [84]:

$$Mn_3O_4 + Li^+ + e^- \rightarrow LiMn_3O_4 \tag{5.6}$$

$$LiMn_3O_4 + Li^+ + e^- \rightarrow 3MnO + Li_2O \tag{5.7}$$

$$MnO + 2Li^+ + 2e^- \leftrightarrow Mn + Li_2O \tag{5.8}$$

$$Mn_3O_4 + 8Li^+ + 8e^- \leftrightarrow 3Mn + 4Li_2O \tag{5.9}$$

As expected, MnO shows the lowest irreversible capacity according to reference [50]; however, due to the high reversibility of the conversion reaction, one could expect a very low irreversible capacity. MnO usually exhibits a first-cycle capacity over 1,100 mAh g^{-1} [50, 61, 86–89], which is much higher than its theoretical capacity. Like Cr_2O_3, this is due to the formation of a thick gel-like layer on the

manganese nanoparticles. A reversible capacity of about 65–70% of the first-cycle capacity is usually observed, which corresponds to the theoretical capacity of MnO. MnO usually exhibits good capacity retention with or without carbon additives. Zhong et al. reported reversible capacities for a MnO/carbon composite of 650 mAh g^{-1} [91].

5.3.3 Iron

Iron oxides are attractive because of the low cost of iron, its environmental friendliness, and its experimental oxidation potential of 1.8 V, which is much lower than cobalt or nickel oxides. Three different iron oxides are available as anode material for lithium-ion batteries, ranging from Fe^{3+} to Fe^{2+}: Fe_2O_3, Fe_3O_4, and FeO. In the 1980s, it was shown by Thackeray and Coetzer that Fe_2O_3 and Fe_3O_4 could react reversibly with a Li/Al alloy in a LiCl-KCl molten salt mixture at 420°C [42]. In this process, α-Fe_2O_3 and Fe_3O_4 were reduced to Fe^0. When discharged at room temperature down to 1 V, the lithium initial insertion in Fe_2O_3 and Fe_3O_4 leads to the creation of lithiated phases $Li_xFe_2O_3$ and $Li_xFe_3O_4$ ($0 \leq x \leq 2$)[92]. It is only recently that the full reduction of iron oxides at room temperature was demonstrated by discharging them down to 5 mV [37]. FeO just goes through the conventional reversible conversion reaction, $FeO + 2Li^+ + 2e^- \leftrightarrow Fe + Li_2O$; this first lithiation occurs at 0.6–0.7 V and yields a first discharge capacity of 1,150 mAh g^{-1} [37]. The oxidation plateau is observed around 1.6 V, and the subsequent reduction plateaus are around 1 V (see Table 5.2). FeO exhibits a reversible capacity of 745 mAh $g^{-1,}$ fading to 300 mAh g^{-1} after 50 cycles. Additional plateaus between 3 and 1 V are observed when using Fe_2O_3 or Fe_3O_4 corresponding to lithium intercalation/deintercalation. In contrast to FeO, which has not been widely investigated, there has been a lot of interest in Fe_2O_3 and Fe_3O_4 as anode materials for lithium-ion batteries. A lot of effort has been put to control the size and morphology of iron oxide particles. It has been reported that micron-sized iron oxides show poor capacity retention [57, 93]. For example, in the case of Fe_2O_3, nanorods [94, 95], nanoflakes [96], and nanotubes [62] were synthesized, while in the case of Fe_3O_4, nanowires [97] and nanospindles [57] were prepared and tested. In both cases, the most stable capacities were obtained when these nanomaterials were coated with carbon, which is explained by the fact that the solid electrolyte interphase (SEI) is created on the carbon rather than on the material itself. After a first discharge capacity of 1,300 mAh g^{-1}, carbon-coated Fe_2O_3 nanotubes yielded a stable capacity of 700 mAh g^{-1} after 150 cycles, compared to 450 mAh g^{-1} for uncoated nanotubes [62]. The same phenomenon was observed for carbon-coated Fe_3O_4 nanowires that showed a stable reversible capacity of 800 mAh g^{-1} over 50 cycles, while their uncoated counterpart performed more poorly, with a reversible capacity of 400 mAh g^{-1} after 50 cycles [97].

Another approach has recently been investigated, that is, growing Fe_3O_4 nanoparticles directly on graphene (exfoliated graphite), and good stability was

obtained [98]. The highly conductive graphene sheets act as an electronic conductor [99] and also as support for the Fe_3O_4 nanoparticles. The reported discharge capacities are 1,400 mAh g^{-1} for the first discharge and 900 mAh g^{-1} for the second discharge, slightly increasing with cycling. The rate capability is also very good with a capacity over 600 mAh g^{-1} at rate slightly over C (1,050 mA g^{-1}). Composite electrodes using single-wall carbon nanotubes (SWCNTs) were shown to improve the cycling performance of Fe_3O_4 [91]. The composite was prepared by the reduction of a precursor of FeOOH nanorods in presence of SWCNTs to yield Fe_3O_4 and prepared as a binder-free electrode with only 5 wt% of SWCNTs. Extremely high capacities were reported, reaching over 1,000 mAh g^{-1} at 1 C rate.

5.3.4 Cobalt

Cobalt oxides, CoO and Co_3O_4, have both been shown to be active toward lithium [23, 37]. They have theoretical capacities over 700 mAh g^{-1}: 715 mAh g^{-1} for CoO and 890 mAh g^{-1} for Co_3O_4. Like other TMOs, cobalt oxides go through a reversible conversion reaction with lithium. The first reduction reaction occurs at about 1.0 V and the subsequent one at about 1.2–1.8 V [17, 38]. The oxidation occurs at potentials ranging from 2.2 to 2.4 V [37], which is too high and is the main drawback for this particular metal oxide. It will lead to a low output cell voltage when used in a full lithium-ion battery; as shown by Badway et al., a $Co_3O_4/LiCoO_2$ cell has an output voltage of only 2 V [100]. However, since cobalt oxides provide a generally high and stable capacity, it is one of the first transition metal oxides to attract interest. While large particles (over 2 μm) of CoO and Co_3O_4 deliver high and stable capacities [38], the performance of nanosized cobalt oxide will depend greatly on their morphology. Co_3O_4 nanowires [101], nanotubes [102], nanoneedles [103], and hollow microspheres [104] give stable capacities above 700 mAh g^{-1} at low cycling rate. CoO nanowires [105] also yield stable capacities over 700 mAh g^{-1} at 1 C. However, Co_3O_4 nanoplatelets [106] showed capacities with drastic drop or large variations depending on heat treatment. Composites of Co_3O_4 with graphene sheets are useful in preventing metal oxide particles agglomeration and the stacking of the graphene sheets [107]. The metal oxide is grown *in situ* on graphene oxide sheets which are then reduced to produce evenly distributed Co_3O_4 nanoparticles. This leads to a stable capacity of 800 mAh g^{-1} over 30 cycles.

5.3.5 Nickel

NiO has been reported as an anode material for lithium-ion batteries. It goes through the conventional reversible conversion reaction with lithium: $NiO + 2Li^+ + 2e^- \leftrightarrow Ni + Li_2O$ [37, 64, 108]. The first lithiation occurs at about 0.6 V, whereas

the subsequent lithiation plateaus slope from 1.0 to 1.4 V. Like cobalt oxides, NiO is in general less attractive due to its higher delithiation potential that ranges from 1.5 to 2.2 V, which would provide a lower cell voltage. In addition, NiO usually shows very poor capacity retention [108–112] unless it is nanostructured [64, 113, 114]. Thin films made of nanoparticles of 30–100 nm particles showed a first discharge capacity ranging from 800 to 850 mAh g^{-1} and a reversible capacity of about 450–500 mAh g^{-1} after 100 cycles with cycling rates ranging from 10 to 80 μA cm^{-2} [113]. Some of the best performance were obtained with NiO nanowalls of 100-nm height and less than 40 nm thick, showing a capacity of 640 mAh g^{-1} after 80 cycles at 1.25 C (900 mA g^{-1}) [64]. However, an irreversible loss of about 40% occurs after the first cycle. Similar data were reported for mesoporous carbon-encapsulated NiO nanocomposite [115].

5.3.6 Copper

As previously mentioned in this chapter, copper oxide has been used as early as 1980 as cathode for primary lithium batteries [39, 40], and more recently as cathode for lithium-ion batteries [41]. Its use as an anode was investigated by Poizot et al. in 2000 and the two phases CuO and Cu_2O have been found to be active toward lithium [37]. Like manganese oxides, copper oxides generally show a large irreversible capacity that ranges from 30% to 50% of the first discharge capacity. In addition, due to the higher molecular weight of copper, and its lower oxidation numbers, copper oxides have lower theoretical specific capacities than other TMOs: 674 mAh g^{-1} for CuO and 375 mAh g^{-1} for Cu_2O. It has been shown that a nanosized material does not always provide the best performance, as shown by Grugeon et al.; 1-μm-sized CuO and Cu_2O provide more stable capacities (400 mAh g^{-1}) than 150-nm particles [116]. However, usually, nanostructured CuO or Cu_2O shows better capacity retention than micrometric particles. For example, nanowires having a diameter of 100 nm provided a first discharge capacity of 1,040 mAh g^{-1} and a reversible capacity of 650 mAh g^{-1} after 100 cycles, which represents an irreversibility of 37% [117]. CuO nanoribbon provided similar results with a reversible capacity of 600 mAh g^{-1} after 280 cycles at C/4 and an irreversibility of about 31% [118]. Good rate capability was also reported: 507 mAh g^{-1} at C/3.4, 417 mAh g^{-1} at C/1.7, and 332 mAh g^{-1} at C/0.85. However, one should be careful with these values since the density of the electrode was only 0.4 mg cm^{-2} [118]. CuO was also studied as urchin-like nanostructures of 100 nm [65]. A stable capacity of 600 mAh g^{-1} was obtained after 50 cycles at C/4.5 along with an irreversible capacity of only 25% of the first discharge capacity.

Since an oxidation number of +1 exists for copper, CuO behaves differently from other TMOs; it first goes through an insertion mechanism with mixed oxidation state, that is, $Cu^{2+}{}_{1-x}Cu^{+}{}_{x}O_{(1-x)/2} (0<x<0.4)$ up to Cu_2O, and then the conventional reversible conversion reaction occurs. Figure 5.7 shows the typical voltage profile of a CuO anode.

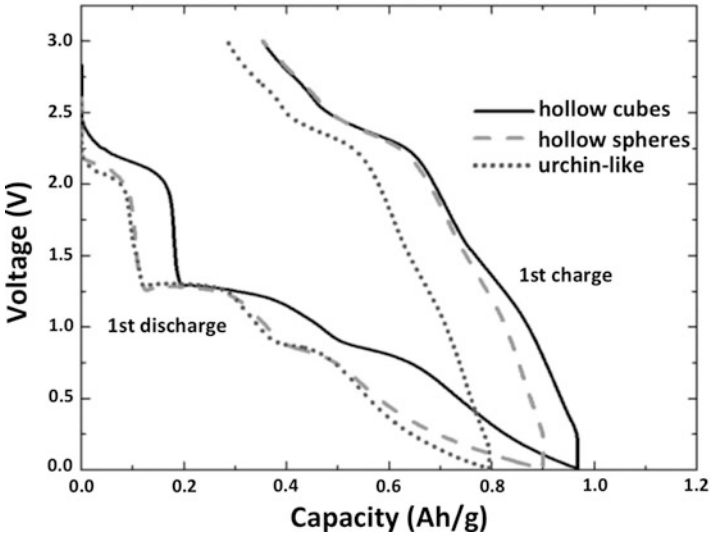

Fig. 5.7 Voltage profile of CuO hollow nanostructures (Reprinted with permission of John Wiley & Sons, Inc. [65])

5.3.7 Zinc

Zinc is a post-transition metal, and like the TMOs, ZnO has an interstice-free würtzite structure that does not allow any lithium insertion. As most TMOs, ZnO reacts with lithium through a reversible conversion reaction [119]. However, as a post-TMO, ZnO behaves quite differently since the *in situ* made zinc nanoparticles further react with lithium by forming a ZnLi alloy [120–122]. As most alloying reaction with lithium, Zinc particles undergo a large volume change during this process, about 163% [119]. This expansion is responsible for the large irreversible capacity observed for the first few cycles. Usually, reversible capacities ranging from 500 mAh g^{-1} [123] to 350 mAh g^{-1} [119] or less [73] with very poor capacity retention upon cycling are observed.

5.4 Mixed Oxides: AB_2O_4

Several compounds containing two TMOs and having a spinel-like structure have been investigated, with A having an oxidation state of +2 and B of +3. Three series have been studied, the manganite (AMn_2O_4), ferrite (AFe_2O_4), and cobaltite (ACo_2O_4).

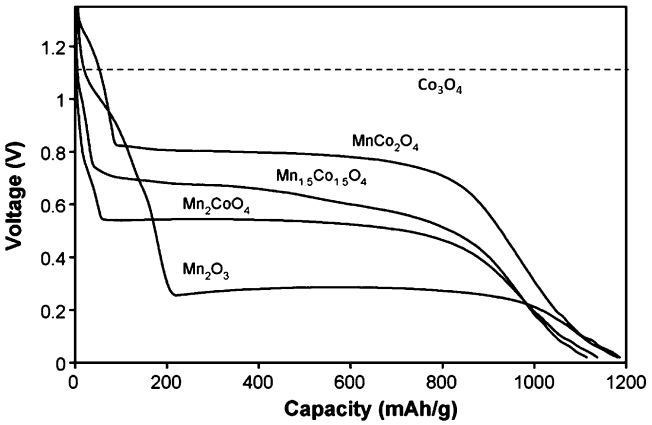

Fig. 5.8 Voltage profile of the first lithiation of $Mn_xCo_{3-x}O_4$ spinel series (with x = 1, 1.5, or 2) and Mn_2O_3 prepared via an ethanol dehydration procedure that precipitates gel-like citrate precursors annealed at 800°C for 24 h. The cells were discharged at 1 C rate (Reprinted from Electrochimica Acta [124]. Copyright (2011), with permission from Elsevier. The voltage plateau value of Co_3O_4 has been taken from reference [125])

In general, their performance is pretty close to the performance of their simple oxides (i.e., Mn_3O_4, Fe_3O_4, and Co_3O_4). Interestingly enough, one would expect two lithiation plateaus corresponding to the two TMs, but only one plateau is experimentally observed for the first lithiation, as shown by Lavela et al. [124] for the $Mn_xCo_{3-x}O_4$ series (x = 0, 1, 1.5, or 2) and Mn_2O_3. Figure 5.8 shows the potential of the first lithiation plateau of this series. It seems that the potential is controlled by the TM content. As expected, Mn_2O_3 exhibits the lowest potential plateau that then shifts to higher values as more cobalt was added into the spinel structure up to Co_3O_4. This is easily explained by the fact that manganese oxides are more difficult to reduce (0.3 V [83]) than cobalt oxides (0.9–1.1 V [100, 125]). The same phenomenon has been observed for $Co_{3-x}Fe_xO_4$ (x = 0, 1, or 2) [125]. Upon the delithiation, the spinel structure is never recovered; instead, a mixture of single TMOs is observed, as demonstrated by Sharma for $ZnCo_2O_4$ [126]; two voltage plateaus are observed afterward.

5.4.1 AMn_2O_4

Manganese-based oxides are very interesting because of their low delithiation voltage plateau; it ranges from 1.0 to 1.4 V (see Fig. 5.1). However, they also show a large irreversibility due to the formation of an unstable gel-like layer on the nanoparticles of the Mn/Li_2O composite material. This manganite series has first

been investigated by Pasero et al. via a brief study of the cycling performance of the off-stoichiometric $Co_{0.4}Mn_{2.6}O_4$. It provides a low but stable capacity of about 400 mAh g^{-1} after 10 cycles, and an irreversibility of about 60% [127]. Unfortunately, no information on the particle size or long-term cycling was provided. We recently reported on the performance of nanoparticles of $NiMn_2O_4$ (10 nm) and $CoMn_2O_4$ (200–500 nm) [73]. We showed that $NiMn_2O_4$ nanoparticles perform well for the first four cycles only. A predicted irreversible capacity of 210 mAh g^{-1} was observed that is due to the oxidation of Mn^0 to Mn^{2+} and not Mn^{3+}. Even though the capacity retention between the second and the fourth discharge is very good, it unfortunately drops drastically below 200 mAh g^{-1} after 20 cycles [73]. This drastic capacity fade could be explained by the adverse reaction of nickel nanoparticles with the electrolyte which leads to a thick ionically resistive organic SEI that does not allow lithium ions to travel through. According to cyclic voltammetry, the nickel reduction and oxidation peaks are drastically reduced in intensity after the tenth cycle. $CoMn_2O_4$ nanoparticles showed better capacity performance with a first discharge capacity of 975 mAh g^{-1} and a reversible capacity of 330 mAh g^{-1} after 50 cycles; however, capacity retention is still an issue [73].

An additional capacity is observed when the post-transition metal zinc is used. $ZnMn_2O_4$ is a good alternative when considering the low oxidation potential of zinc and manganese nanoparticles: 1.2 and 1.5 V, respectively [73]. These values will potentially increase the battery output voltage. In addition, their price and toxicity are lower compared to nickel and cobalt; they are abundant and environmentally friendly. Three groups reported the performance of $ZnMn_2O_4$ [73, 128]. In the first case it was synthesized via polymer-pyrolysis method, the obtained nanoparticles (30–60 nm) showed a capacity value of 626 mAh g^{-1} over 50 cycles [128, 129]. In the second case, $ZnMn_2O_4$ nanoflake-shaped particles prepared via calcination of an agglomerated Zn-Mn citrate complex precursor provided capacity values of 650 mAh g^{-1} at 100 mA g^{-1} [130]. In the third case, $ZnMn_2O_4$ particles were prepared via decomposition of a precipitate of zinc and manganese oxalate. We showed that it is necessary to investigate the effect of the size of the particles on the performance of the battery (see Fig. 5.5). An optimum particle size ranging from 75 to 150 nm provided a capacity of 690 mAh g^{-1} after 70 cycles, which represents 88% capacity retention. Good rate capability has also been observed for this material: 170 mAh g^{-1} at 3 C.

5.4.2 AFe_2O_4

Even though iron exhibits a higher oxidation potential than manganese, some members of the AFe_2O_4 series (A = Co, Ni, Cu, or Zn) have shown interesting performance. However, these compounds still exhibit large irreversible capacities ranging from 35% to 60% [125, 131–134] with capacity values of 600–800 mAh g^{-1} for $CoFe_2O_4$ [131], 600 mAh g^{-1} or less for $NiFe_2O_4$ [131, 133], and 550 mAh g^{-1}

for $CuFe_2O_4$ [134]. Even though an extra capacity is added by using zinc, $ZnFe_2O_4$ nanoparticles (100–300 nm) show a stable reversible capacity of only 615 mAh g^{-1} which still represents an irreversible capacity of 46% [135].

5.4.3 ACo_2O_4

Because of the cobalt content, compounds from the ACo_2O_4 (A = Mn, Fe, Ni, Cu, or Zn) series show higher delithiation potentials than spinels from the two other series [126]. The first member of the series, $MnCo_2O_4$ does not show good performance with a capacity of only 400 mAh g^{-1} after 50 cycles, which represents an irreversibility of 65% [124]. Depending on the preparation method, $FeCo_2O_4$ performed quite well with a good capacity retention with values ranging from 630 to 750 mAh g^{-1} after 50 cycles, which represents an irreversibility of 45% and 35%, respectively [125, 136]. Nanoparticles of $NiCo_2O_4$/C nanocomposite (10–20 nm) provided a capacity of 715 mAh g^{-1} after 50 cycles that decays significantly with cycling; an irreversibility of about 40% was measured [137]. Nanoparticles of $CuCo_2O_4$ (10–20 nm) showed a stable capacity of 745 mAh g^{-1} after 50 cycles, which represents an irreversibility of only 38% [138]. For the last member of the series, an extra capacity is added using zinc. $ZnCo_2O_{4r}$ nanoparticles (15–20 nm) showed a very stable capacity of 900 mAh g^{-1} after 60 cycles and an irreversible capacity that represents only 25% [126]. Other groups also reported very stable capacity values: 750 mAh g^{-1} for $ZnCo_2O_4$ nanoflakes [139] and up to 1,200 mAh g^{-1} for $ZnCo_2O_4$ nanowires (100–300 nm in diameter), but for 20 cycles only [140].

5.5 TMXs with X = S, N, P, and F

In the previous sections, we have shown that lithiation and delithiation potentials can be tuned by changing the transition metal. Another possibility is to use mixed oxides such as AB_2O_4 spinels with A and B being two different TMs. In this case, the potential can be tuned, but however occurs only during the first lithiation reaction, as shown by Fig. 5.8. For the subsequent delithiations, the active material is composed of a mixture of both oxides; the latter then reacts at two different potentials. Another solution for tuning lithiation and delithiation potentials is to change the anion. The previous sections focused on oxides, while this section will deal with fluorides, sulfides, nitrides, and phosphides, which will be referred to as TMFs, TMSs, TMNs, and TMPs respectively. They react with lithium the same way as TMOs and form a matrix of LiF, Li_2S, Li_3N, and Li_3P, respectively. For the same transition metal, the following trend is usually observed when looking at the lithiation potential of the different TMXs: TMFs > TMSs > TMOs > TMNs > TMPs. This observation is actually related to the decrease in the M-X bond polarization when going from M-F to M-P.

Due to the very high ionicity of the metal-fluorine chemical bond, very high oxidation and reduction potentials are observed for TMFs. The electronegativity difference between most transition metals and fluorine ranges from 2.5 to 2.1, which makes the TMFs more attractive as cathodes than anodes, especially FeF_3. The higher reduction potential related to the higher ionicity of the metal-fluorine chemical bond makes the conversion reaction possible even with titanium and vanadium [59], which was something impossible for TMOs. FeF_3 is one of the TMFs that shows the highest theoretical capacity (712 mAh g^{-1}); it also provides the best battery performance [141]. Other TMFs, such as NiF_2, CuF_2, CoF_2 and MnF_2, and MnF_3, do not show any good long-term capacity retention [45, 69].

TMSs were initially used as cathode material for primary cells (e.g.,TiS_2, FeS_2) [142–144]. Recently, it has been shown that TMSs can also go through a conversion reaction that is reversible to some extent. As shown in Tables 5.2 and 5.3, in general, TMSs show higher oxidation potentials than TMOs, which means that the reduction of the metal is easier but that the oxidation is more difficult. For

Table 5.3 Summary table of electromotive forces, reduction and oxidation potentials, and theoretical capacities of TMFs, TMSs, TMNs, and TMPs

TM	X	Phase	EMF[b] [45] (V)	E first reduction (V vs. Li/Li^+)	E second reduction (V vs. Li/Li^+)	E oxidation (V vs. Li/Li^+)	Number of Li per metal	Theoretical specific capacity [45] (mAh g^{-1})
Ti		TiF_3 [59]	1.396	1.5/1.0–0.5	1.2–1.0	1.7–2.2	3	767
		TiS_2	1.233	–	–	–	4	957
V		VF_3 [59]	1.863	0.3	1.8/1.0/0.1	0.1/2.5	3	745
		VN	–	–	–	–	3	1,239
Cr		CrF_3 [141]	–	1.7	1.9	2.6	3	738
		CrN [156]	–	[a]	[a]	1/2.7[a]	3	1,218
Mn		MnF_2	1.919	–	–	–	2	577
		MnF_3	2.647	–	–	–	3	719
		MnS [157]	1.144	–	0.7	1.2	2	616
		MnS_2	1.692	–	–	–	4	900
		Mn_4N	0.083	–	–	–	0.75	459
		Mn_5N_2	0.176	–	–	–	1.2	531
		MnP_4 [151]	–	0.65/0.1	0.78/0.1	1.2/1.56	12	1,798
Fe		FeF_2	2.664	–	–	–	2	571
		FeF_3 [141]	2.742	3.0/2.0	2.1/3.1	2.8/3.3	3	712
		FeS	1.747	–	–	–	2	610
		FeS_2[158]	1.861	1.5	2.0/1.5[a]	1.9/2.5[a]	4	893
		Fe_4N	0.432	–	–	–	0.75	339
		Fe_3N [148]	–	2.0/1.8	0.9	1.5–2.2[a]	1	443
		FeP [56]	–	0.1	0.5/0.2	1	3	926
		FeP_2 [56, 153]	–	0.25	0.7	1.1	6	1,365

(continued)

Table 5.3 (continued)

TM	X	Phase	EMF[b] [45] (V)	E first reduction (V vs. Li/Li^+)	E second reduction (V vs. Li/Li^+)	E oxidation (V vs. Li/Li^+)	Number of Li per metal	Theoretical specific capacity [45] (mAh g^{-1})
Co		CoF_2	2.854	–	–	–	2	553
		CoF_3	3.617	–	–	–	3	694
		$CoS_{0.9}$ [52]	–	1.1	1.4	2	1.8	545
		CoS_2 [159]	1.898	1.6/1.4[a]	1.9/1.4[a]	2/2.3	4	871
		Co_3S_4	1.644	–	–	–	2.7	703
		CoN [150]	–	0.6/0.25[a]	0.8/0.3[a]	0.7 and up[a]	3	1,103
		Co_3N [148]	0.326	1.1/0.8[a]	1.5–1.7[a]	2.1	1	421
		CoP [154]	–	From 0.9 and down[a]	0.6	1	3	894
		CoP_3 [155]	–	0.3	0.7	1.1	9	1,588
Ni		NiF_2 [45]	2.964	1.5	2.5[a]	1.4/3.2	2	554
		NiS [52]	–	1.2–0.8	1.8/1.4	2.8/2	2	591
		NiS_2 [160]	–	1.7–1.3[a]	1.8/1.4	2.1	4	873
		Ni_3N [161]	–	0.55	1.7–0.7[a]	1.5/2.1[a]	1	423
		NiP_2 [152]	–	0.5–0.2[a]	0.7	1.2	6	1,332
		NiP_3 [54]	–	0.6	0.75	1.2	9	1,590
Cu		CuF_2 [45]	3.553	2.1/1.2	3–0[a]	0–4[a]	2	528
		CuS [52]	1.998	2.1/1.6	2.1/1.6[a]	2.3	2	561
		Cu_2S	1.827	–	–	–	1	337
		Cu_3N [162]	–	0.5 and less[a]	–	1.7	1	393
		CuP_2 [163]	–	0.6	0.8	1.1	6	1,284
Zn		ZnF_2	2.404	–	–	–	3	778

[a]Slope
[b]EMF: Electromotive force

example, the first lithiation occurs at a voltage plateau of 0.7 V for MnS versus 0.2 V for MnO. As for lithium-sulfur batteries [145, 146], the main issue with TMSs (Li_2S) is the dissolution of sulfur species in the carbonate electrolytes, which means that the reversibility of the reaction is jeopardized at each discharge. Better performance is obtained when using either all solid-state batteries or a polymer electrolyte such as polyethylene oxide: lithium salt at 80°C [147].

Nitrides usually show lower potentials than oxides [148, 149]. It has been reported that TMNs can also go through the reversible conversion reaction process starting from vanadium. Nitrides show high first discharge capacity; however, they do not show very good capacity retention except for CoN that has a capacity over 700 mAh g^{-1} [150].

TMPs are probably the next most interesting TMX anode materials after TMOs since they exhibit the lowest delithiation potentials of all investigated TMXs. The metal-phosphorus bond shows a very strong covalent bond that is more difficult to

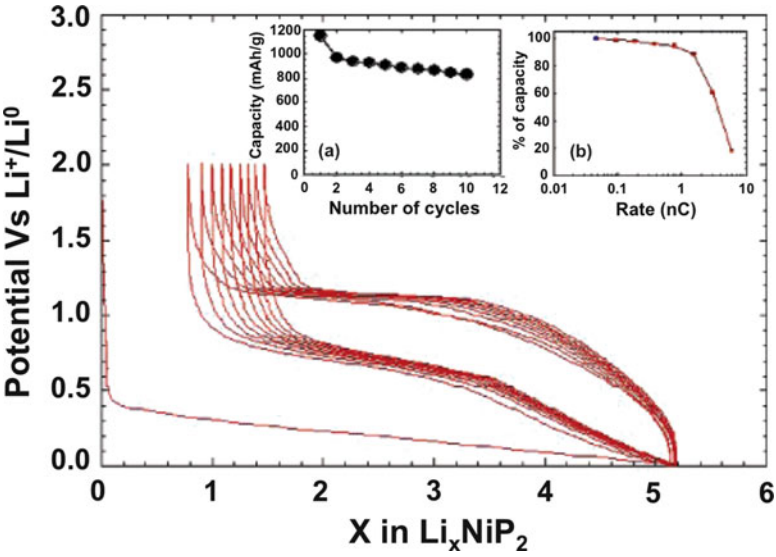

Fig. 5.9 Voltage profile for a foam-NiP_2/Li cell at C/10 from 2 to 0 V at a C/2 rate with, as insets, (**a**) its corresponding capacity retention and (**b**) rate capability performance of a foam-NiP_2 electrode measured, for reasons of current density associated to Li-metal, in a lithium-ion-type configuration using $LiFePO_4$ as the positive electrode (Reprinted with permission from [152]. Copyright (2011) American Chemical Society)

break than an ionic bond [151, 152]. As a matter of fact, only transition metals starting from manganese can be reduced. In addition, due to their high phosphorus content and the uptake of three lithium ions per phosphorus atom, they exhibit high theoretical capacities (see Table 5.3). As shown in Table 5.3, MnP_4 shows optimal potentials and a high theoretical capacity of 1,798 mAh g^{-1}. Unfortunately, the efficiency of the conversion reaction process is quite low as shown by Gillot et al. [145]. FeP and FeP_2 exhibit very low delithiation potential of about 1.1 V. During their first lithiation, they almost reach their theoretical capacity values, which are over 900 mAh g^{-1} [56, 153]. After 100 cycles at C/10, FeP still shows a capacity of 300 mAh g^{-1} [56]. Whereas CoO showed very high delithiation potential over 2 V, its phosphide counterparts CoP and CoP_3 show a much lower delithiation potential of about 1.1 V [154, 155]. CoP_3 almost reaches its theoretical capacity during the first lithiation; however, capacity retention is still an issue. As shown by Figs. 5.9 and 5.10, NiP_2 and NiP_3 are also of interest, especially because of their low delithiation potentials (1.2 V, see Table 5.3) and also their flat lithiation and delithiation plateaus [54, 152]. In addition, they have theoretical specific capacities over 1,300 mAh g^{-1}. During the first lithiation, NiP_2 reaches the theoretical value and still has a capacity of 850 mAh g^{-1} after 10 cycles and also shows good rate capability up to 1 C [152].

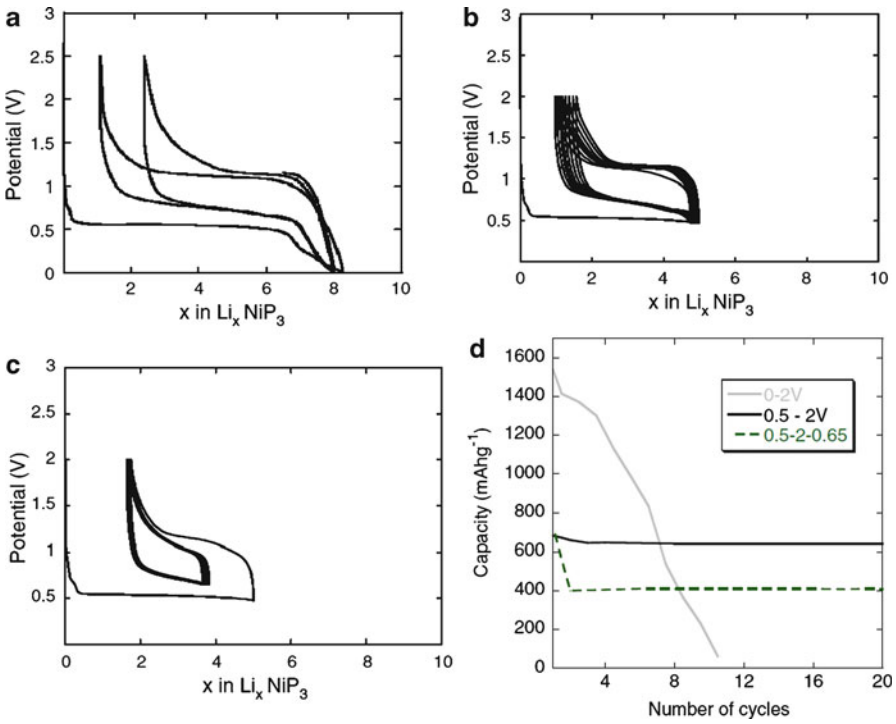

Fig. 5.10 Voltage profiles for a NiP_3/Li cell cycled at a C/10 rate between (**a**) 2.5 and 0 V, (**b**) 2 and 0.5 V, and (**c**) 0.5, 2, and 0.65 V. (**d**) The capacity retention at a C/10 rate for a NiP_3/Li cell cycled between 2 and 0 V (in *gray line*), 2 and 0.5 V (in *black line*), and between 2 and 0.5 V in the first discharge and 2 and 0.65 in the further cycles (in *dotted line*) (With kind permission from Springer Science + Business Media: Ionics [52] (2011))

5.6 Summary and Outlook

Due to the increasing demand for high energy density lithium-ion batteries, R&D laboratories around the world are actively looking for high specific capacity anode materials. In this regard TMOs, among others, have been of much interest. TMOs (and TMXs in general) having low oxidation number transition metals react in an unusual way with lithium. They undergo a reversible conversion reaction with at least two electrons or more exchanged per TM atom. This reaction also involves the reversible formation and decomposition of a Li_2O matrix. The conversion reaction is reversible only because TMOs are reduced into an intimate mixture of nanoparticles of transition metals and Li_2O. This reversible solid-state reaction does not occur at a macroscopic scale. This chapter also showed that the particle size and particle morphology of the starting material are crucial for the battery performance; each TMO has an optimum particle size and morphology. The large

hysteresis observed between the charge and the discharge potential profile curve is one of the major issues with TMOs. However, it improves after the first lithiation, since the second lithiation potential is higher than the first. The delithiation potential of the anode is crucial for LIBs since it will set the output cell voltage; the lower the value, the higher the cell output voltage. TMOs generally show high delithiation voltages. One way to tune this voltage plateau is to change the transition metal, the lowest one being chromium and manganese around 1.4 V and the iron around 1.8 V. Another way would be to use TMOs made of a mix of two different transition metals, such as $CoMn_2O_4$, in order to have an average potential. This strategy works well for the first lithiation, but however does not work for the subsequent lithiation/delithiation since a mixture of both oxides is then obtained. The last strategy to change the voltage plateaus is to change the oxide counterions to fluorides, sulfides, nitrides, and phosphides. TMFs show the highest delithiation potentials and are more interesting as cathodes, while TMPs provide the lowest delithiation potentials, so potentially the highest output cell voltage of all TMXs.

References

1. Ravet N, Goodenough J, Besner S, Simoneau M, Hovington P, Armand M (1999) Improved iron based cathode material. In: Electrochemical society meeting abstracts, 99(2):Abstract #127
2. Huang H, Yin SC, Nazar LF (2001) Approaching theoretical capacity of $LiFePO_4$ at room temperature at high rates. Electrochem Solid State Lett 4(10):A170–A172
3. Armand M, Gauthier M, Magnan J-F, Ravet N (2002) Method for synthesis of carbon-coated redox materials with controlled size. Patent number: WO 02/27823, PCT/CA01/01349
4. Yabuuchi N, Ohzuku T (2003) Novel lithium insertion material of $LiCo_{1/3}Ni_{1/3}Mn_{1/3}O_2$ for advanced lithium-ion batteries. J Power Sources 119–121:171–174
5. Belharouak I, Lu W, Vissers D, Amine K (2006) Safety characteristics of Li $(Ni_{0.8}Co_{0.15}Al_{0.05})O_2$ and $Li(Ni_{1/3}Co_{1/3}Mn_{1/3})O_2$. Electrochem Commun 8(2):329–335
6. Weaving JS, Coowar F, Teagle DA, Cullen J, Dass V, Bindin P, Green R, Macklin WJ (2001) Development of high energy density Li-ion batteries based on $LiNi_{1-x-y}Co_xAl_yO_2$. J Power Sources 97–98:733–735
7. Primak W, Fuchs LH (1954) Electrical conductivities of natural graphite crystals. Phys Rev 95(1):22
8. Inoue H (2006) High capacity negative-electrode materials next to carbon; Nexelion. In: International meeting on lithium batteries, Biarritz
9. Mizutani S, Inoue H (2005) Negative active material and method for production thereof, non-aqueous electrolyte secondary cell using the same. Patent number: 2005-0208378
10. Kawakami S, Asao M (2005) Electrode material for anode of rechargeable lithium battery, electrode structural body using said electrode material, rechargeable lithium battery using said electrode structural body, process for producing said electrode structural body, and process for producing said rechargeable lithium battery. Patent number: 6,949,312
11. Dahn JR, Mar RE, Abouzeid A (2006) Combinatorial study of $Sn_{1-x}Co_x$ ($0 < x < 0.6$) and $[Sn_{0.55}Co_{0.45}]_{1-y}C_y$ ($0 < y < 0.5$) alloy negative electrode materials for Li-ion batteries. J Electrochem Soc 153(2):A361–A365

12. Hassoun J, Ochal P, Panero S, Mulas G, Bonatto Minella C, Scrosati B (2008) The effect of CoSn/$CoSn_2$ phase ratio on the electrochemical behaviour of $Sn_{40}Co_{40}C_{20}$ ternary alloy electrodes in lithium cells. J Power Sources 180(1):568–575
13. Hassoun J, Mulas G, Panero S, Scrosati B (2007) Ternary Sn-Co-C Li-ion battery electrode material prepared by high energy ball milling. Electrochem Commun 9(8):2075–2081
14. Ferguson PP, Todd ADW, Dahn JR (2008) Comparison of mechanically alloyed and sputtered tin-cobalt-carbon as an anode material for lithium-ion batteries. Electrochem Commun 10(1):25–31
15. Hassoun J, Panero S, Mulas G, Scrosati B (2007) An electrochemical investigation of a Sn-Co-C ternary alloy as a negative electrode in Li-ion batteries. J Power Sources 171(2):928–931
16. SonyCorporation (2011) Sony, the market for notebook PC; development of a tin-based amorphous anode, for high-capacity rechargeable lithium-ion battery 3.5Ah: the "Nexelion" (trans). Accessed January, 2012. Available from http://www.sony.co.jp/SonyInfo/News/Press/201107/11-078/
17. Ohzuku T, Ueda A, Yamamoto N (1995) Zero-strain insertion material of $Li[Li_{1/3}Ti_{5/3}]O_4$ for rechargeable lithium cells. J Electrochem Soc 142(5):1431–1435
18. Amatucci GG, Badway F, Pasquier AD, Zheng T (2001) An asymmetric hybrid nonaqueous energy storage cell. J Electrochem Soc 148(8):A930–A939
19. Thackeray MM, Goodenough JB (1985) Solid state cell wherein an anode, solid electrolyte and cathode each comprise a cubic-close-packed framework structure. Patent number: 4,504,371
20. Guerfi A, Sévigny S, Lagacé M, Hovington P, Kinoshita K, Zaghib K (2003) Nano-particle $Li_4Ti_5O_{12}$ spinel as electrode for electrochemical generators. J Power Sources 119–121:88–94
21. Plitz I, DuPasquier A, Badway F, Gural J, Pereira N, Gmitter A, Amatucci GG (2006) The design of alternative nonaqueous high power chemistries. Appl Phys Mater Sci Process 82(4):615–626
22. Du Pasquier A (2008) Nanosized titanium oxides for energy storage and conversion. In: Eftekhari A (ed) Nanostructured materials in electrochemistry. Wiley-VCH, Weinheim, pp 387–408
23. Nazri G-A, Pistoia G (2004) Lithium batteries: science and technology. Kluwer, Boston, 708 pages
24. Hamon Y, Brousse T, Jousse F, Topart P, Buvat P, Schleich DM (2001) Aluminum negative electrode in lithium ion batteries. J Power Sources 97–98:185–187
25. Rao BML, Francis RW, Christopher HA (1977) Lithium-aluminum electrode. J Electrochem Soc 124(10):1490–1492
26. Li J, Lewis RB, Dahn JR (2007) Sodium carboxymethyl cellulose. Electrochem Solid State Lett 10(2):A17–A20
27. Kasavajjula U, Wang C, Appleby AJ (2007) Nano- and bulk-silicon-based insertion anodes for lithium-ion secondary cells. J Power Sources 163(2):1003–1039
28. Chan CK, Peng H, Liu G, McIlwrath K, Zhang XF, Huggins RA, Cui Y (2008) High-performance lithium battery anodes using silicon nanowires. Nat Nanotechnol 3(1):31–35
29. Yang J, Winter M, Besenhard JO (1996) Small particle size multiphase Li-alloy anodes for lithium-ion batteries. Solid State Ion 90(1–4):281–287
30. Derrien G, Hassoun J, Panero S, Scrosati B (2007) Nanostructured Sn-C composite as an advanced anode material in high-performance lithium-ion batteries. Adv Mater 19(17):2336–2340
31. Nara H, Fukuhara Y, Takai A, Komatsu M, Mukaibo H, Yamauchi Y, Momma T, Kuroda K, Osaka T (2008) Cycle and rate properties of mesoporous tin anode for lithium ion secondary batteries. Chem Lett 37(2):142–143
32. Balbuena PB, Wang Y (2004) Lithium-ion batteries: solid-electrolyte interphase. Imperial College Press, London

33. Li H, Huang X, Chen L, Wu Z, Liang Y (1999) A high capacity nano-Si composite anode material for lithium rechargeable batteries. Electrochem Solid State Lett 2(11):547–549
34. Beattie SD, Larcher D, Morcrette M, Simon B, Tarascon JM (2008) Si electrodes for Li-ion batteries – a new way to look at an old problem. J Electrochem Soc 155(2):A158–A163
35. Buqa H, Holzapfel M, Krumeich F, Veit C, Novák P (2006) Study of styrene butadiene rubber and sodium methyl cellulose as binder for negative electrodes in lithium-ion batteries. J Power Sources 161(1):617–622
36. Kovalenko I, Zdyrko B, Magasinski A, Hertzberg B, Milicev Z, Burtovyy R, Luzinov I, Yushin G (2011) A major constituent of brown algae for use in high-capacity Li-ion batteries. Science 334(6052):75–79
37. Poizot P, Laruelle S, Grugeon S, Dupont L, Tarascon JM (2000) Nano-sized transition-metal oxides as negative-electrode materials for lithium-ion batteries. Nature 407:496–499
38. Cabana J, Monconduit L, Larcher D, Palacín MR (2010) Beyond intercalation-based Li-ion batteries: the state of the art and challenges of electrode materials reacting through conversion reactions. Adv Mater 22:E170–E192
39. Iijima T, Toyoguchi Y, Nishimura J, Ogawa H (1980) Button-type lithium battery using copper oxide as a cathode. J Power Sources 5(1):99–109
40. Novák P (1985) CuO cathode in lithium cells–II. Reduction mechanism of CuO. Electrochim Acta 30(12):1687–1692
41. Li T, Ai XP, Yang HX (2011) Reversible electrochemical conversion reaction of Li_2O/CuO nanocomposites and their application as high-capacity cathode materials for Li-ion batteries. J Phys Chem C 115(13):6167–6174
42. Thackeray MM, Coetzer J (1981) A preliminary investigation of the electrochemical performance of α-Fe_2O_3 and Fe_3O_4 cathodes in high-temperature cells. Mater Res Bull 16(5):591–597
43. Brousse T, Crosnier O, Santos-Peña J, Sandu I, Fragnaud P, Schleich DM (2002) Recent progress in the development of tin-based negative electrodes for Li-ion batteries. In: Kumagai N, Komaba S (eds) Materials chemistry in lithium batteries. Research Signpost, Kerala
44. Li H, Huang X, Chen L (1999) Anodes based on oxide materials for lithium rechargeable batteries. Solid State Ion 123(1–4):189–197
45. Li H, Balaya P, Maier J (2004) Li-storage via heterogeneous reaction in selected binary metal fluorides and oxides. J Electrochem Soc 151(11):A1878–A1885
46. Jamnik J, Maier J (2003) Nanocrystallinity effects in lithium battery materials: aspects of nano-ionics. Part IV. Phys Chem Chem Phys 5(23):5215–5220
47. Thackeray MM (1997) Manganese oxides for lithium batteries. Prog Solid State Chem 25(1–2):1–71
48. Binotto G, Larcher D, Prakash AS, Herrera Urbina R, Hegde MS, Tarascon JM (2007) Synthesis, characterization, and Li-electrochemical performance of highly porous Co_3O_4 659 powders. Chem Mater 19(12):3032–3040
49. Larcher D, Sudant G, Leriche J-B, Chabre Y, Tarascon J-M (2002) The electrochemical reduction of Co_3O_4 in a lithium cell. J Electrochem Soc 149(3):A234–A241
50. Fang X, Lu X, Guo X, Mao Y, Hu Y-S, Wang J, Wang Z, Wu F, Liu H, Chen L (2010) Electrode reactions of manganese oxides for secondary lithium batteries. Electrochem Commun 12(11):1520–1523
51. Debart A, Dupont L, Poizot P, Leriche J-B, Tarascon JM (2001) A transmission electron microscopy study of the reactivity mechanism of tailor-made CuO particles toward lithium. J Electrochem Soc 148(11):A1266–A1274
52. Débart A, Dupont L, Patrice R, Tarascon JM (2006) Reactivity of transition metal (Co, Ni, Cu) sulphides versus lithium: the intriguing case of the copper sulphide. Solid State Sci 8(6):640–651
53. Crosnier O, Nazar LF (2004) Facile reversible displacement reaction of Cu_3P with lithium at low potential. Electrochem Solid State Lett 7(7):A187–A189

54. Boyanov S, Gillot F, Monconduit L (2008) The electrochemical reactivity of the NiP_3 skutterudite-type phase with lithium. Ionics 14(2):125–130
55. Larcher D, Masquelier C, Bonnin D, Chabre Y, Masson V, Leriche J-B, Tarascon J-M (2003) Effect of particle size on lithium intercalation into α-Fe_2O_3. J Electrochem Soc 150(1): A133–A139
56. Boyanov S, Bernardi J, Gillot F, Dupont L, Womes M, Tarascon JM, Monconduit L, Doublet ML (2006) FeP: another attractive anode for the Li-ion battery enlisting a reversible two-step insertion/conversion process. Chem Mater 18(15):3531–3538
57. Zhang W-M, Wu X-L, Hu J-S, Guo Y-G, Wan L-J (2008) Carbon coated Fe_3O_4 nanospindles as a superior anode material for lithium-ion batteries. Adv Funct Mater 18(24):3941–3946
58. Dupont L, Laruelle S, Grugeon S, Dickinson C, Zhou W, Tarascon JM (2008) Mesoporous Cr_2O_3 as negative electrode in lithium batteries: TEM study of the texture effect on the polymeric layer formation. J Power Sources 175(1):502–509
59. Li H, Richter G, Maier J (2003) Reversible formation and decomposition of LiF clusters using transition metal fluorides as precursors and their application in rechargeable Li batteries. Adv Mater 15(9):736–739
60. Hu J, Li H, Huang X (2005) Cr_2O_3-based anode materials for Li-ion batteries. Electrochem Solid State Lett 8(1):A66–A69
61. Sun B, Chen Z, Kim H-S, Ahn H, Wang G (2010) MnO/C core-shell nanorods as high capacity anode materials for lithium-ion batteries. J Power Sources 196(6):3346–3349
62. Liu J, Li Y, Fan H, Zhu Z, Jiang J, Ding R, Hu Y, Huang X (2010) Iron oxide-based nanotube arrays derived from sacrificial template-accelerated hydrolysis: large-area design and reversible lithium storage. Chem Mater 22(1):212–217
63. Wang G, Liu T, Xie X, Ren Z, Bai J, Wang H (2011) Structure and electrochemical performance of Fe_3O_4/graphene nanocomposite as anode material for lithium-ion batteries. Mater Chem Phys 128(3):336–340
64. Varghese B, Reddy MV, Yanwu Z, Lit CS, Hoong TC, Subba Rao GV, Chowdari BVR, Wee ATS, Lim CT, Sow C-H (2008) Fabrication of NiO nanowall electrodes for high performance lithium ion battery. Chem Mater 20(10):3360–3367
65. Park JC, Kim J, Kwon H, Song H (2009) Gram-scale synthesis of Cu_2O nanocubes and subsequent oxidation to CuO hollow nanostructures for lithium-ion battery anode materials. Adv Mater 21(7):803–807
66. Gao XP, Bao JL, Pan GL, Zhu HY, Huang PX, Wu F, Song DY (2004) Preparation and electrochemical performance of polycrystalline and single crystalline CuO nanorods as anode materials for Li ion battery. J Phys Chem B 108(18):5547–5551
67. Xiang J, Tu J, Huang X, Yang Y (2008) A comparison of anodically grown CuO nanotube film and Cu_2O film as anodes for lithium ion batteries. J Solid State Electrochem 12(7):941–945
68. Xiang JY, Tu JP, Yuan YF, Huang XH, Zhou Y, Zhang L (2009) Improved electrochemical performances of core-shell Cu_2O/Cu composite prepared by a simple one-step method. Electrochem Commun 11(2):262–265
69. Liu J, Li Y, Ding R, Jiang J, Hu Y, Ji X, Chi Q, Zhu Z, Huang X (2009) Carbon/ZnO nanorod array electrode with significantly improved lithium storage capability. J Phys Chem C 113(13):5336–5339
70. Lee J-H, Hon M-H, Chung Y-W, Leu I-C (2010) The effect of TiO_2 coating on the electrochemical performance of ZnO nanorod as the anode material for lithium-ion battery. Appl Phys A Mater Sci Process 102(3):545–550
71. Hu J, Li H, Huang X, Chen L (2006) Improve the electrochemical performances of Cr_2O_3 anode for lithium ion batteries. Solid State Ion 177(26–32):2791–2799
72. Balaya P, Li H, Kienle L, Maier J (2003) Fully reversible homogeneous and heterogeneous Li storage in RuO_2 with high capacity. Adv Funct Mater 13:621–625

73. Courtel FM, Duncan H, Abu-Lebdeh Y, Davidson IJ (2011) High capacity anode materials for Li-ion batteries based on spinel metal oxides AMn_2O_4 (A = Co, Ni, and Zn). J Mater Chem 21(27):10206–10218
74. Yuan Z, Huang F, Feng C, Sun J, Zhou Y (2003) Synthesis and electrochemical performance of nanosized Co_3O_4. Mater Chem Phys 79(1):1–4
75. Oh SW, Bang HJ, Bae YC, Sun Y-K (2007) Effect of calcination temperature on morphology, crystallinity and electrochemical properties of nano-crystalline metal oxides (Co_3O_4, CuO, and NiO) prepared via ultrasonic spray pyrolysis. J Power Sources 173(1):502–509
76. Maier J (2007) Mass storage in space charge regions of nano-sized systems (nano-ionics. Part V). Faraday Discuss 134:51–56
77. Balaya P, Bhattacharyya AJ, Jamnik J, Zhukovskii YF, Kotomin EA, Maier J (2006) Nano-ionics in the context of lithium batteries. J Power Sources 159(1):171–178
78. Dupont L, Grugeon S, Laruelle S, Tarascon JM (2007) Structure, texture and reactivity versus lithium of chromium-based oxides films as revealed by TEM investigations. J Power Sources 164(2):839–848
79. Anisimov VI, Korotin MA, Kurmaev EZ (1990) Band-structure description of Mott insulators (NiO, MnO, FeO, CoO). J Phys Condens Matter 2(17):3973–3987
80. Jiang L-Y, Xin S, Wu X-L, Li H, Guo Y-G, Wan L-J (2010) Non-sacrificial template synthesis of Cr_2O_3-C hierarchical core/shell nanospheres and their application as anode materials in lithium-ion batteries. J Mater Chem 20(35):7565–7569
81. Grugeon S, Laruelle S, Dupont L, Chevallier F, Taberna PL, Simon P, Gireaud L, Lascaud S, Vidal E, Yrieix B, Tarascon M (2005) Combining electrochemistry and metallurgy for new electrode designs in Li-ion batteries. Chem Mater 17(20):5041–5047
82. Liu X, Yasuda H, Yamachi M (2005) Solid solution of nickel oxide and manganese oxide as negative active material for lithium secondary cells. J Power Sources 146(1–2):510–515
83. Cai Y, Liu S, Yin X, Hao Q, Zhang M, Wang T (2010) Facile preparation of porous one-dimensional Mn_2O_3 nanostructures and their application as anode materials for lithium-ion batteries. Physica E 43(1):70–75
84. Gao J, Lowe MA, Abruna HD (2011) Spongelike nanosized Mn_3O_4 as a high-capacity anode material for rechargeable lithium batteries. Chem Mater 23(13):3223–3227
85. Wang H, Cui L-F, Yang Y, Sanchez Casalongue H, Robinson JT, Liang Y, Cui Y, Dai H (2010) Mn_3O_4-graphene hybrid as a high-capacity anode material for lithium ion batteries. J Am Chem Soc 132(40):13978–13980
86. Yu XQ, He Y, Sun JP, Tang K, Li H, Chen LQ, Huang XJ (2009) Nanocrystalline MnO thin film anode for lithium ion batteries with low overpotential. Electrochem Commun 11(4):791–794
87. Zhong K, Xia X, Zhang B, Li H, Wang Z, Chen L (2010) MnO powder as anode active materials for lithium ion batteries. J Power Sources 195(10):3300–3308
88. Zhong K, Zhang B, Luo S, Wen W, Li H, Huang X, Chen L (2010) Investigation on porous MnO microsphere anode for lithium ion batteries. J Power Sources 196(16):6802–6808
89. Liu J, Pan Q (2010) MnO/C nanocomposites as high capacity anode materials for Li-ion batteries. Electrochem Solid State Lett 13(10):A139–A142
90. Ren Y, Armstrong AR, Jiao F, Bruce PG (2010) Influence of size on the rate of mesoporous electrodes for lithium batteries. J Am Chem Soc 132(3):996–1004
91. Zhong K, Xia X, Zhang B, Li H, Wang Z, Chen L (2010) MnO powder as anode active materials for lithium ion batteries. J Power Sources 195(10):3300–3308
92. Thackeray MM, David WIF, Goodenough JB (1982) Structural characterization of the lithiated iron oxides $Li_xFe_3O_4$ and $Li_xFe_2O_3$ ($0 < x < 2$). Mater Res Bull 17(6):785–793
93. Ban C, Wu Z, Gillaspie DT, Chen L, Yan Y, Blackburn JL, Dillon AC (2010) Nanostructured Fe_3O_4/SWNT electrode: binder-free and high-rate Li-ion anode. Adv Mater 22(20): E145–E149

94. Song Y, Qin S, Zhang Y, Gao W, Liu J (2010) Large-scale porous hematite nanorod arrays: direct growth on titanium foil and reversible lithium storage. J Phys Chem C 114(49):21158–21164
95. Tartaj P, Amarilla JM (2011) Iron oxide porous nanorods with different textural properties and surface composition: preparation, characterization and electrochemical lithium storage capabilities. J Power Sources 196(4):2164–2170
96. Chun L, Wu X, Lou X, Zhang Y (2010) Hematite nanoflakes as anode electrode materials for rechargeable lithium-ion batteries. Electrochim Acta 55(9):3089–3092
97. Muraliganth T, Vadivel Murugan A, Manthiram A (2009) Facile synthesis of carbon-decorated single-crystalline Fe_3O_4 nanowires and their application as high performance anode in lithium ion batteries. Chem Commun 47:7360–7362
98. Zhou G, Wang D-W, Li F, Zhang L, Li N, Wu Z-S, Wen L, Lu GQ, Cheng H-M (2010) Graphene-wrapped Fe_3O_4 anode material with improved reversible capacity and cyclic stability for lithium ion batteries. Chem Mater 22(18):5306–5313
99. Zhu Y, Murali S, Cai W, Li X, Suk JW, Potts JR, Ruoff RS (2010) Graphene and graphene oxide: synthesis, properties, and applications. Adv Mater 22:3906–3924
100. Badway F, Plitz I, Grugeon S, Laruelle S, Dolle M, Gozdz AS, Tarascon JM (2002) Metal oxides as negative electrode materials in Li-ion cells. Electrochem Solid State Lett 5(6): A115–A118
101. Li Y, Tan B, Wu Y (2008) Mesoporous Co_3O_4 nanowire arrays for lithium ion batteries with high capacity and rate capability. Nano Lett 8(1):265–270
102. Du N, Zhang H, Chen BD, Wu JB, Ma XY, Liu ZH, Zhang YQ, Yang DR, Huang XH, Tu JP (2007) Porous Co_3O_4 nanotubes derived from $Co_4(CO)_{12}$ clusters on carbon nanotube templates: a highly efficient material for Li-battery applications. Adv Mater 19(24):4505–4509
103. Lou XW, Deng D, Lee JY, Archer LA (2008) Thermal formation of mesoporous single-crystal Co_3O_4 nano-needles and their lithium storage properties. J Mater Chem 18(37):4397–4401
104. Wang X, Wu X-L, Guo Y-G, Zhong Y, Cao X, Ma Y, Yao J (2010) Synthesis and lithium storage properties of Co_3O_4 nanosheet-assembled multishelled hollow spheres. Adv Funct Mater 20(10):1680–1686
105. Jiang J, Liu J, Ding R, Ji X, Hu Y, Li X, Hu A, Wu F, Zhu Z, Huang X (2009) Direct synthesis of CoO porous nanowire arrays on Ti substrate and their application as lithium-ion battery electrodes. J Phys Chem C 114(2):929–932
106. Wang J, Du G, Zeng R, Niu B, Chen Z, Guo Z, Dou S (2010) Porous Co_3O_4 nanoplatelets by self-supported formation as electrode material for lithium-ion batteries. Electrochim Acta 55(16):4805–4811
107. Wu Z-S, Ren W, Wen L, Gao L, Zhao J, Chen Z, Zhou G, Li F, Cheng H-M (2010) Graphene anchored with Co_3O_4 nanoparticles as anode of lithium ion batteries with enhanced reversible capacity and cyclic performance. ACS Nano 4(6):3187–3194
108. Wang Y, Qin Q-Z (2002) A nanocrystalline NiO thin-film electrode prepared by pulsed laser ablation for Li-ion batteries. J Electrochem Soc 149(7):A873–A878
109. Hosono E, Fujihara S, Honma I, Zhou H (2006) The high power and high energy densities Li ion storage device by nanocrystalline and mesoporous Ni/NiO covered structure. Electrochem Commun 8(2):284–288
110. Needham SA, Wang GX, Liu HK (2006) Synthesis of NiO nanotubes for use as negative electrodes in lithium ion batteries. J Power Sources 159(1):254–257
111. Wang H, Pan Q, Wang X, Yin G, Zhao J (2009) Improving electrochemical performance of NiO films by electrodeposition on foam nickel substrates. J Appl Electrochem 39(9):1597–1602
112. Liu L, Li Y, Yuan S, Ge M, Ren M, Sun C, Zhou Z (2009) Nanosheet-based NiO microspheres: controlled solvothermal synthesis and lithium storage performances. J Phys Chem C 114(1):251–255

113. Nuli Y-N, Zhao S-L, Qin Q-Z (2003) Nanocrystalline tin oxides and nickel oxide film anodes for Li-ion batteries. J Power Sources 114(1):113–120
114. Pan Q, Liu J (2009) Facile fabrication of porous NiO films for lithium-ion batteries with high reversibility and rate capability. J Solid State Electrochem 13(10):1591–1597
115. Cheng M-Y, Hwang B-J (2010) Mesoporous carbon-encapsulated NiO nanocomposite negative electrode materials for high-rate Li-ion battery. J Power Sources 195(15):4977–4983
116. Grugeon S, Laruelle S, Herrera-Urbina R, Dupont L, Poizot P, Tarascon J-M (2001) Particle size effects on the electrochemical performance of copper oxides toward lithium. J Electrochem Soc 148(4):A285–A292
117. Chen LB, Lu N, Xu CM, Yu HC, Wang TH (2009) Electrochemical performance of polycrystalline CuO nanowires as anode material for Li ion batteries. Electrochim Acta 54(17):4198–4201
118. Ke F-S, Huang L, Wei G-Z, Xue L-J, Li J-T, Zhang B, Chen S-R, Fan X-Y, Sun S-G (2009) One-step fabrication of CuO nanoribbons array electrode and its excellent lithium storage performance. Electrochim Acta 54(24):5825–5829
119. Wang H, Pan Q, Cheng Y, Zhao J, Yin G (2009) Evaluation of ZnO nanorod arrays with dandelion-like morphology as negative electrodes for lithium-ion batteries. Electrochim Acta 54(10):2851–2855
120. Dey AN (1971) Electrochemical alloying of lithium in organic electrolytes. J Electrochem Soc 118(10):1547–1549
121. Xiao L, Yang Y, Yin J, Li Q, Zhang L (2009) Low temperature synthesis of flower-like $ZnMn_2O_4$ superstructures with enhanced electrochemical lithium storage. J Power Sources 194(2):1089–1093
122. Wang J, King P, Huggins RA (1986) Investigations of binary lithium-zinc, lithium-cadmium and lithium-lead alloys as negative electrodes in organic solvent-based electrolyte. Solid State Ion 20(3):185–189
123. Zhang CQ, Tu JP, Yuan YF, Huang XH, Chen XT, Mao F (2007) Electrochemical performances of Ni-coated ZnO as an anode material for lithium-ion batteries. J Electrochem Soc 154(2):A65–A69
124. Lavela P, Tirado JL, Vidal-Abarca C (2007) Sol-gel preparation of cobalt manganese mixed oxides for their use as electrode materials in lithium cells. Electrochim Acta 52(28):7986–7995
125. Lavela P, Ortiz GF, Tirado JL, Zhecheva E, Stoyanova R, Ivanova S (2007) High-performance transition metal mixed oxides in conversion electrodes: a combined spectroscopic and electrochemical study. J Phys Chem C 111(38):14238–14246
126. Sharma Y, Sharma N, Subba Rao GV, Chowdari BVR (2007) Nanophase $ZnCo_2O_4$ as a high performance anode material for Li-ion batteries. Adv Funct Mater 17(15):2855–2861
127. Pasero D, Reeves N, West AR (2005) Co-doped Mn_3O_4: a possible anode material for lithium batteries. J Power Sources 141(1):156–158
128. Xiao L, Yang Y, Yin J, Li Q, Zhang L (2009) Low temperature synthesis of flower-like $ZnMn_2O_4$ superstructures with enhanced electrochemical lithium storage. J Power Sources 194(2):1089–1093
129. Yang Y, Zhao Y, Xiao L, Zhang L (2008) Nanocrystalline $ZnMn_2O_4$ as a novel lithium-storage material. Electrochem Commun 10(8):1117–1120
130. Deng Y, Tang S, Zhang Q, Shi Z, Zhang L, Zhan S, Chen G (2011) Controllable synthesis of spinel nano-$ZnMn_2O_4$ via a single source precursor route and its high capacity retention as anode material for lithium ion batteries. J Mater Chem 21(32):11987–11995
131. Lavela P, Tirado JL (2007) $CoFe_2O_4$ and $NiFe_2O_4$ synthesized by sol-gel procedures for their use as anode materials for Li ion batteries. J Power Sources 172(1):379–387
132. Chu Y-Q, Fu Z-W, Qin Q-Z (2004) Cobalt ferrite thin films as anode material for lithium ion batteries. Electrochim Acta 49(27):4915–4921

133. Alcántara R, Jaraba M, Lavela P, Tirado JL, Jumas JC, Olivier-Fourcade J (2003) Changes in oxidation state and magnetic order of iron atoms during the electrochemical reaction of lithium with $NiFe_2O_4$. Electrochem Commun 5(1):16–21
134. Bomio M, Lavela P, Tirado JL (2007) Fe Mössbauer spectroscopy and electron microscopy study of metal extraction from $CuFe_2O_4$ electrodes in lithium cells. Chemphyschem 8:1999–2007
135. Sharma Y, Sharma N, Rao GVS, Chowdari BVR (2008) Li-storage and cyclability of urea combustion derived $ZnFe_2O_4$ as anode for Li-ion batteries. Electrochim Acta 53(5):2380–2385
136. Sharma Y, Sharma N, Subba Rao GV, Chowdari BVR (2008) Studies on spinel cobaltites, $FeCo_2O_4$ and $MgCo_2O_4$ as anodes for Li-ion batteries. Solid State Ion 179(15–16):587–597
137. NuLi Y, Zhang P, Guo Z, Liu H, Yang J (2008) $NiCo_2O_4$/C nanocomposite as a highly reversible anode material for lithium-ion batteries. Electrochem Solid State Lett 11(5): A64–A67
138. Sharma Y, Sharma N, Rao GVS, Chowdari BVR (2007) Lithium recycling behaviour of nano-phase-$CuCo_2O_4$ as anode for lithium-ion batteries. J Power Sources 173(1):495–501
139. Qiu Y, Yang S, Deng H, Jin L, Li W (2010) A novel nanostructured spinel $ZnCo_2O_4$ electrode material: morphology conserved transformation from a hexagonal shaped nanodisk precursor and application in lithium ion batteries. J Mater Chem 20(21):4439–4444
140. Du N, Xu Y, Zhang H, Yu J, Zhai C, Yang D (2011) Porous $ZnCo_2O_4$ nanowires synthesis via sacrificial templates: high-performance anode materials of Li-ion batteries. Inorg Chem 50(8):3320–3324
141. Plitz I, Badway F, Al-Sharab J, DuPasquier A, Cosandey F, Amatucci GG (2005) Structure and electrochemistry of carbon-metal fluoride nanocomposites fabricated by solid-state redox conversion reaction. J Electrochem Soc 152(2):A307–A315
142. Gabano JP, Dechenaux V, Gerbier G, Jammet J (1972) D-size lithium cupric sulfide cells. J Electrochem Soc 119(4):459–461
143. Whittingham MS (1978) Chemistry of intercalation compounds: metal guests in chalcogenide hosts. Prog Solid State Chem 12(1):41–99
144. Henriksen GL, Jansen AN (2002) Lithium batteries. In: Linden D, Reddy TB (eds) Handbook of batteries. McGraw-Hill, New York
145. Ellis BL, Lee KT, Nazar LF (2010) Positive electrode materials for Li-ion and Li-batteries. Chem Mater 22(3):691–714
146. Ji X, Lee KT, Nazar LF (2009) A highly ordered nanostructured carbon-sulphur cathode for lithium-sulphur batteries. Nat Mater 8(6):500–506
147. Han S-C, Kim K-W, Ahn H-J, Ahn J-H, Lee J-Y (2003) Charge-discharge mechanism of mechanically alloyed NiS used as a cathode in rechargeable lithium batteries. J Alloys Compd 361(1–2):247–251
148. Fu Z-W, Wang Y, Yue X-L, Zhao S-L, Qin Q-Z (2004) Electrochemical reactions of lithium with transition metal nitride electrodes. J Phys Chem B 108(7):2236–2244
149. Huggins RA (2002) Alternative materials for negative electrodes in lithium systems. Solid State Ion 152–153:61–68
150. Das B, Reddy MV, Malar P, Osipowicz T, Subba Rao GV, Chowdari BVR (2009) Nanoflake CoN as a high capacity anode for Li-ion batteries. Solid State Ion 180(17–19):1061–1068
151. Gillot F, Monconduit L, Doublet ML (2005) Electrochemical behaviors of binary and ternary manganese phosphides. Chem Mater 17(23):5817–5823
152. Gillot F, Boyanov S, Dupont L, Doublet ML, Morcrette M, Monconduit L, Tarascon JM (2005) Electrochemical reactivity and design of NiP_2 negative electrodes for secondary Li-ion batteries. Chem Mater 17(25):6327–6337
153. Silva DCC, Crosnier O, Ouvrard G, Greedan J, Safa-Sefat A, Nazar LF (2003) Reversible lithium uptake by FeP_2. Electrochem Solid State Lett 6(8):A162–A165
154. Zhang Z, Yang J, Nuli Y, Wang B, Xu J (2005) CoP_x synthesis and lithiation by ball-milling for anode materials of lithium ion cells. Solid State Ion 176(7–8):693–697

155. Pralong V, Souza DCS, Leung KT, Nazar LF (2002) Reversible lithium uptake by CoP_3 at low potential: role of the anion. Electrochem Commun 4(6):516–520
156. Sun Q, Fu Z-W (2007) An anode material of CrN for lithium-ion batteries. Electrochem Solid State Lett 10(8):A189–A193
157. Zhang N, Yi R, Wang Z, Shi R, Wang H, Qiu G, Liu X (2008) Hydrothermal synthesis and electrochemical properties of alpha-manganese sulfide submicrocrystals as an attractive electrode material for lithium-ion batteries. Mater Chem Phys 111(1):13–16
158. Montoro LA, Rosolen JM (2003) Gelatin/DMSO: a new approach to enhancing the performance of a pyrite electrode in a lithium battery. Solid State Ion 159(3–4):233–240
159. Yan JM, Huang HZ, Zhang J, Liu ZJ, Yang Y (2005) A study of novel anode material CoS_2 for lithium ion battery. J Power Sources 146(1–2):264–269
160. Takeuchi T, Sakaebe H, Kageyama H, Sakai T, Tatsumi K (2008) Preparation of NiS_2 using spark-plasma-sintering process and its electrochemical properties. J Electrochem Soc 155(9): A679–A684
161. Wang Y, Fu Z-W, Yue X-L, Qin Q-Z (2004) Electrochemical reactivity mechanism of Ni_3N with lithium. J Electrochem Soc 151(4):E162–E167
162. Pereira N, Dupont L, Tarascon JM, Klein LC, Amatucci GG (2003) Electrochemistry of Cu_3N with lithium. J Electrochem Soc 150(9):A1273–A1280
163. Wang K, Yang J, Xie J, Wang B, Wen Z (2003) Electrochemical reactions of lithium with CuP_2 and $Li_{1.75}Cu_{1.25}P_2$ synthesized by ballmilling. Electrochem Commun 5(6):480–483